EGG-TFBP-5146

May 1980

# REACTIVITY INITIATED ACCIDENT TEST SERIES

# TEST RIA 1-4

# QUICK LOOK REPORT

Z. R. Martinson
S. K. Fukuda
D. J. Osetek

M. S. El-Genk
R. E. LaPointe



U.S. Department of Energy
Idaho Operations Office • Idaho National Engineering Laboratory

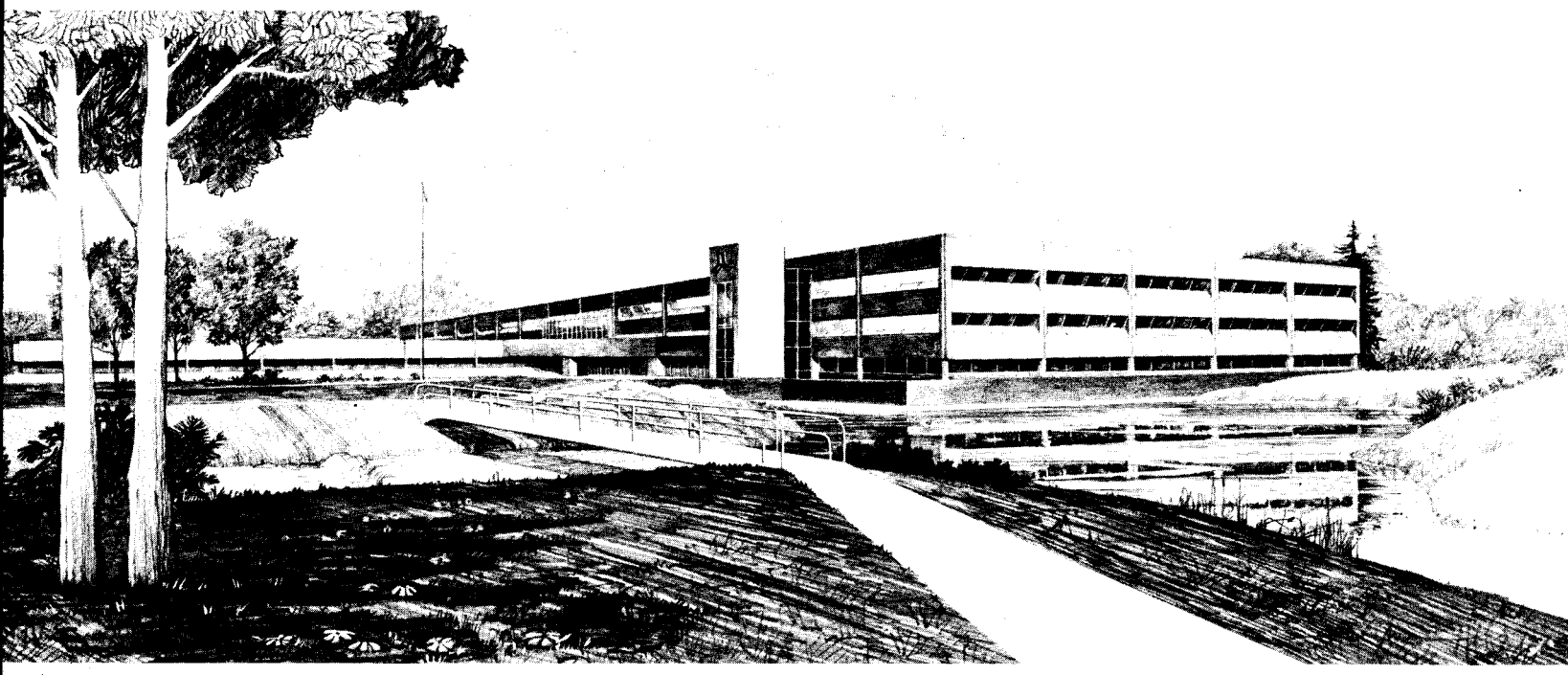

**This is an informal report intended for use as a preliminary or working document**

Prepared for the
U.S. Nuclear Regulatory Commission
Under DOE Contract No. DE-AC07-76ID01570
FIN No. A6041

---

EG&G Idaho, Inc.

FORM EG&G-398
(Rev. 11-79)

MASTER

# INTERIM REPORT

EGG-TFBP--5146

TI85 014373

**Contract Program or Project Title:** Thermal Fuels Behavior Program

**Subject of this Document:** Reactivity Initiated Accident Test Series Test RIA 1-4 Quick Look Report

**Type of Document:** Quick Look Report

**Author(s):** Z. R. Martinson, M. S. El-Genk, S. K. Fukuda, R. E. LaPointe, and D. J. Osetek

**Date of Document:** May 1980

**Responsible NRC Individual and NRC Office or Division:** M. L. Picklesimer

This document was prepared primarily for preliminary or internal use. It has not received full review and approval. Since there may be substantive changes, this document should not be considered final.

EG&G Idaho, Inc.
Idaho Falls, Idaho **83415**

Prepared for the
U.S. Nuclear Regulatory Commission
Washington, D.C.
Under DOE Contract No. **DE-AC07-76ID01570**
NRC FIN No. A6041



INTERIM REPORT

# REACTIVITY INITIATED ACCIDENT TEST SERIES
# TEST RIA 1-4
# QUICK LOOK REPORT

By

Z. R. Martinson
M. S. El-Genk
S. K. Fukuda
R. E. LaPointe
D. J. Osetek

May 1980

R. K. McCardell, Manager
Experiment Specification and Analysis Branch

P. E. MacDonald, Manager
Light Water Reactor Fuel Research Division

## DISCLAIMER

ACKNOWLEDGMENT

The author extend their thanks to D. E. Schwieder and E. C. Odell for their contributions to this report.

CONTENTS



FIGURES

TABLES

## SUMMARY

The third of six planned tests in the Reactivity Initiated Accident (RIA) Test Series I, Test RIA 1-4, was completed April 16, 1980. The specific objective of Test RIA 1-4 was to provide information regarding loss-of-coolable fuel rod geometry following a RIA event for a peak fuel enthalpy equivalent to the present NRC licensing criteria of 280 cal/g $UO_2$.

The test consisted of a nine-rod bundle of pressurized water reactor-type fuel rods previously irradiated to burnups of about 5300 MWd/t. None of the fuel rods were opened prior to the test. After a power calibration and conditioning phase, the fuel rods were subjected to a single power burst that deposited a total fuel energy of about 355 cal/g $UO_2$ at the axial flux peak of the corner rods. The calculated peak fuel enthalpy for this energy insertion was 281 cal/g $UO_2$. Preliminary data from the test indicated that the coolant flow through the shroud stopped for 0.5 s following the power burst, increased to the initial pre power burst flow rate followed by a permanent decrease to about 50% of the initial flow rate about 20 s following the power burst. The Fission Product Detection System indicated fuel rod failure had occurred. The maximum measured cladding temperature was 1625 K. A 1.9 MPa coolant pressure pulse above the initial system pressure of 6.45 MPa was measured. It is believed that all nine fuel rods failed as predicted, but hot cell examination will be required to confirm the extent of fuel rod failure.

# 1. INTRODUCTION

The Reactivity Initiated Accident (RIA) Test RIA 1-4, the first 9-rod fuel rod bundle RIA Test to be performed at BWR hot startup conditions, was completed on April 16, 1980. The test was performed in the Power Burst Facility (PBF), which is operated by the Thermal Fuels Behavior Program of EG&G Idaho, Inc., as a part of the Nuclear Regulatory Commissions Fuel Behavior Program. The specific objective for Test RIA 1-4 was to provide information regarding loss-of-coolable fuel rod geometry following a RIA event for a peak fuel enthalpy equivalent to the present licensing criteria of 280 cal/g.

The most severe RIA is the postulated Boiling Water Reactor (BWR) control rod drop during reactor startup. Therefore the test was conducted at BWR hot startup coolant conditions (538 K, 6.45 MPa, 0.8 l/sec). The test assembly consisted of a 3x3 array of preirradiated fuel rods. The nine fuel rods contained 5.7% enriched $UO_2$ in zircaloy-4 cladding irradiated to an average burnup of 5300 MWd/t.

The test sequence began with steady state power operation to condition the fuel, establish a short-lived fission product inventory, and calibrate the calorimetric measurements and core power chambers, neutron flux and gamma flux detectors. The test train was removed from the in-pile tube (IPT) to replace one of the fuel rods with a nominally identical irradiated rod and twelve flux wire monitors. A 2.8 ms period power burst was then performed that resulted in a peak fuel enthalpy of 281 cal/g $UO_2$ at the axial flux peak of the corner fuel rods, 258 cal/g $UO_2$ in the side rods, and 232 cal/g $UO_2$ in the center rod. Coolant flow measurements were made before and after the power burst to characterize the flow blockage that occurred as a result of fuel rod failure.

Section 2 provides a brief description of test design. Section 3 outlines the "as performed" test conduct, presenting results of the power calibration phase and the estimated magnitude of the power burst. Test results for the power burst phase are presented in Section 4 and, where

applicable, are compared with experiment predictions. In Section 5 the flow blockage measurements and analysis are presented. In Section 6, a brief discussion of the fission product detection system measurements shortly after the power burst is provided. Section 7 presents the conclusions reached from Test RIA 1-4.

It should be noted that all of the data presented in this report are preliminary and have not yet been qualified.

## 2. EXPERIMENT DESIGN

Test RIA 1-4 was comprised of a 9 rod bundle of preirradiated MAPI[a] fuel rods contained in a zircaloy flow shroud. Four axially spaced grid spacers form a 3x3 fuel rod array. A support structure, termed the test assembly centered the rod bundle and flow shroud inside the PBF IPT. The design of the fuel rods, flow shroud support structure and instrumentation are presented in the section.

### 2.1 Fuel Rods and Flow Shroud

A total of ten 5.7 wt% enriched unopened MAPI fuel rods previously irradiated to an average burnup of approximately 5300 MWd/t were used. The nine fuel rods in the 3x3 array for the power calibration and conditioning phase are designated as Rods 804-1, 804-2, 804-3, 804-4, 804-5, 804-6, 804-7, 804-8, and 804-9. The tenth rod designated 804-10, was used as a replacement for 804-2 in the bundle after the power calibration and conditioning test phase was completed. The specific information on rod designations, fuel enrichment, average burnup, internal gas composition and internal pressure for each of the rods is presented in Table 1. The

---

a. The MAPI fuel rods were built by the Westinghouse Electric Company and were irradiated in the Saxton reactor for the Mitsubishi Atomic Power Industries, Inc. Tokyo, Japan.

TABLE 1. SPECIFICATIONS FOR INDIVIDUAL FUEL RODS FOR TEST RIA 1-4

| Rod Number | Original Westinghouse Number | Fuel Enrichment (wt% 235 U) | Average Burnup (MWd/t) | Original 235 U Weight g/rod | Backfill Gas Composition | Backfill Pressure (MPa) |
|---|---|---|---|---|---|---|
| 804-1 | M-55 | 5.7 | 6090 | 27.0 | Air | 0.103 |
| 804-2 | M-30 | 5.7 | 4440 | 27.0 | Air | 0.103 |
| 804-3 | M-34 | 5.7 | 5500 | 27.0 | Air | 0.103 |
| 804-4 | M-29 | 5.7 | 4950 | 27.0 | Air | 0.103 |
| 804-5 | M-62 | 5.7 | 5450 | 27.0 | Air | 0.103 |
| 804-6 | M-38 | 5.7 | 5050 | 27.0 | Air | 0.103 |
| 804-7 | M-41 | 5.7 | 5930 | 27.0 | Air | 0.103 |
| 804-8 | M-40 | 5.7 | 4720 | 27.0 | Air | 0.103 |
| 804-9 | M-61 | 5.7 | 5650 | 27.0 | Air | 0.103 |
| 804-10 | M-32 | 5.7 | 4390 | 27.0 | Air | 0.103 |

as-fabricated nominal design characteristics of these fuel rods are given in Table 2. Fuel Rods 804-1, 804-5 and 804-6 were instrumented with two cladding thermocouples each, as described in Subsection 2.3.

The nine-rod bundle of test rods was positioned within a zircaloy flow shroud (see Figure 1). The fuel rods were positioned in the flow shroud by a series of four grid spacers with a rod-to-rod pitch of 14.3 mm. The grid spacers were centered at 15, 320, 625, and 930 mm above the bottom of the fuel region.

## 2.2 Test Assembly

The test rod bundle, flow shroud and associated instrumentation were held in place in the IPT of the PBF by a support structure referred to as a test assembly. The test assembly consisted of a hanger rod which connected the test bundle to the IPT closure head. A fine mesh fragment screen was located between the test rods and the PBF IPT outlet to prevent fuel and cladding fragments from being dispersed throughout the IPT in the event of fuel rod failure.

## 2.3 Instrumentation

The instrumentation for Test RIA 1-4 was designed to provide information for use in the calorimetric calculation of the rod bundle power during steady state operation, provide an indication of time the cladding was in film boiling, and provide information on the coolant pressure pulse generated during the power burst.

### 2.3.1 Fuel Rod Instrumentation

Fuel Rods 804-1, 804-5 and 804-6 were each instrumented with two cladding surface thermocouples. The other six fuel rods were uninstrumented. The cladding surface thermocouples were titanium sheathed, Type S thermocouples with spaded junctions. The thermocouples were resistance welded to the cladding outer surface. The axial elevation,

TABLE 2.

NOMINAL DESIGN CHARACTERISTICS FOR TEST RIA 1-4 FUEL RODS

| Characteristic [a] | MAPI |
|---|---|
| **Fuel** | |
| Material | $UO_2$ |
| Pellet OD (mm) | 8.59 |
| Pellet length (mm) | 15.2 |
| Pellet enrichment (wt%) | 5.7 |
| Density (% TD)[b] | 94 |
| Fuel stack length (m) | 0.914 |
| End configuration | dished |
| **Cladding** | |
| Material | zircaloy-4 |
| Tube OD (mm) | 9.99 |
| Tube wall thickness (mm minimum) | 0.572 |
| Yield strength (MPa) | 570 |
| Ultimate strength (MPa) | 700 |
| **Fuel Rod** | |
| Gas plenum length (mm) | 45.7 |
| Insulator pellets | none |
| Backfill gas composition | air |
| Backfill pressure (MPa) | 0.103 |
| **Flow Shroud** | |
| Cross Section Flow Area ($m^2$) | 0.001348 |
| Wetted Perimeter (m) | 0.454 |

a. Data are preirradiation values.
b. Theoretical density (TD) of $UO_2$ (10.97 $g/cm^3$).

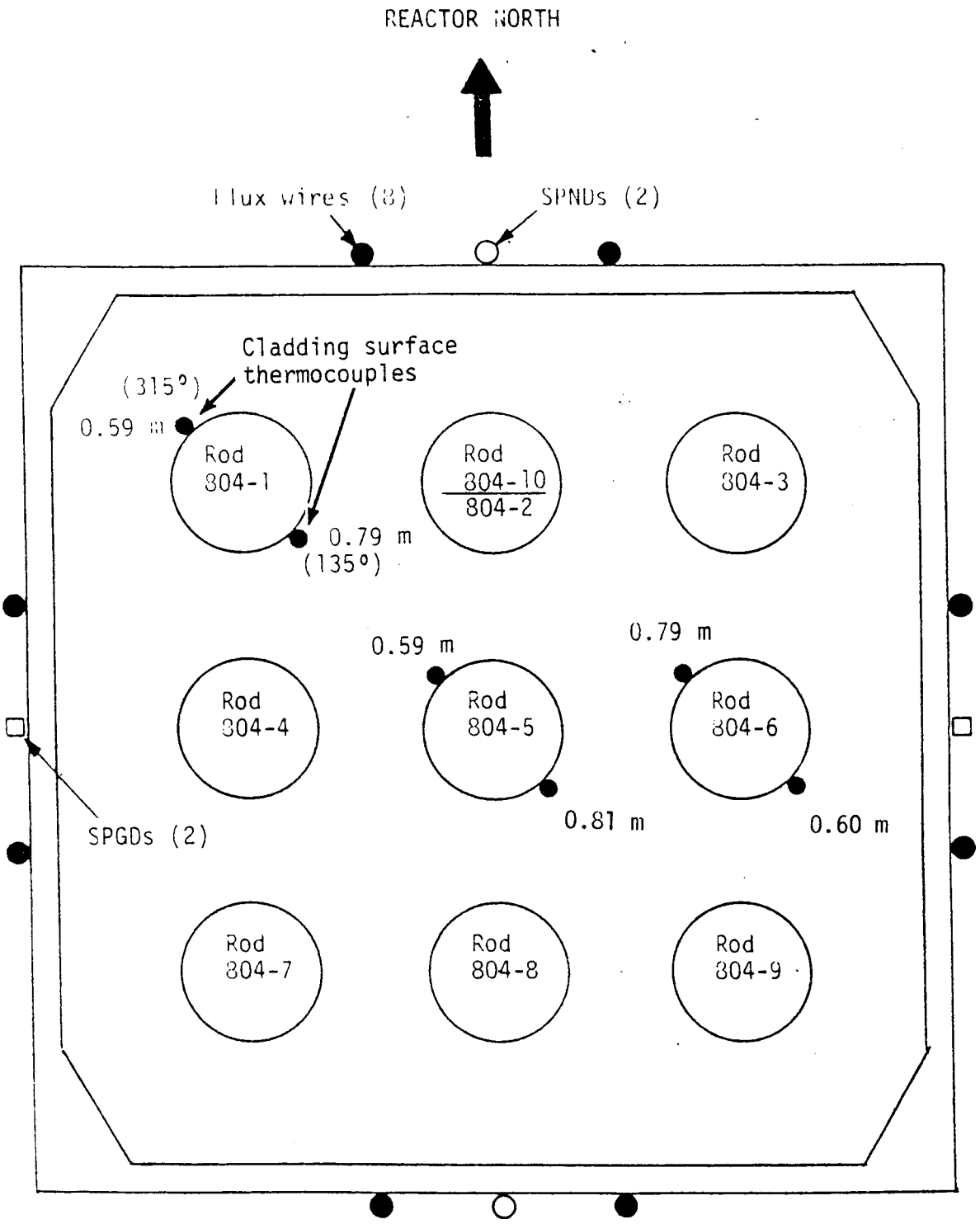


Figure 1. Flow shroud and fuel rod instrumentation.

measured from the bottom of the fuel stack, and the circumferential orientations of the thermocouples are as shown in Figure 1.

### 2.3.2 Test Assembly Instrumentation

The test assembly instrumentation consisted of the following:

1. Two EG&G Idaho, Inc., 69 MPa pressure transducers for measuring large pressure pulses. One transducer is located near the flow shroud outlet and the other is located near the shroud inlet.

2. Two EG&G Idaho, Inc., 17.2 MPa pressure transducers, one located near the shroud outlet for the measurement of normal system pressure and the other transducer is connected by tubing to the flow shroud wall at 452 mm above the bottom of the fuel stack.

3. Two Flow Technology bi-directional flow turbine meters located in tandem at the flow shroud inlet.

4. Four EG&G Idaho, Inc., Type K thermocouples located at the flow shroud inlet to measure the coolant inlet temperature.

5. Two EG&G Idaho, Inc., Type K thermocouples located at the flow shroud outlet to measure the coolant outlet temperature.

6. Two EG&G Idaho, Inc., Type K thermocouples attached to the outer wall of the flow shroud at 0 and 180 degree orientations to measure shroud temperature.

7. Eight removable (0.51% cobalt-99.49% aluminum) flux wires positioned vertically (two per side) on each of the four outer surfaces of the coolant flow shroud to measure the time averaged neutron flux during the power calibration and conditioning phase.

8. Eight removable (100% cobalt) flux wires positioned vertically (two per side) on each of the four outer surfaces of the coolant flow shroud to measure the time averaged neutron flux during the power burst.

9. Two Reuter-Stokes cobalt self-powered neutron detectors (SPNDs), one each located at, 0 and 180 degrees on the outer surface of the coolant flow shroud, to measure the relative neutron flux for use in correlating reactor power to the calibrated fuel rod power.

10. Eight pairs of Copper-Constantan, Type T differential thermocouples positioned at the inlet and outlet of the coolant flow shroud to measure the temperature rise across the shroud.

11. Two Reuter-Stokes platinum self-powered gamma detectors (SPGDs), one each located at 90 and 270 degrees on the outer surface of the coolant flow shroud, to measure the relative gamma flux.

The schematic in Figure 2 is a representation of the Test RIA 1-4 test train. The relative positions of the test assembly instrumentation are also shown in this figure.

### 2.3.3 Plant Instrumentation

Plant instrument data recorded on the data acquisition systems were as follows:

1. NMS-3, NMS-4 ion chambers

2. PPS-1, PPS-2, PPS-3, PPS-4 ion chambers

3. TR-1, TR-2 ion chambers

4. EV-1, EV-2 ion chambers

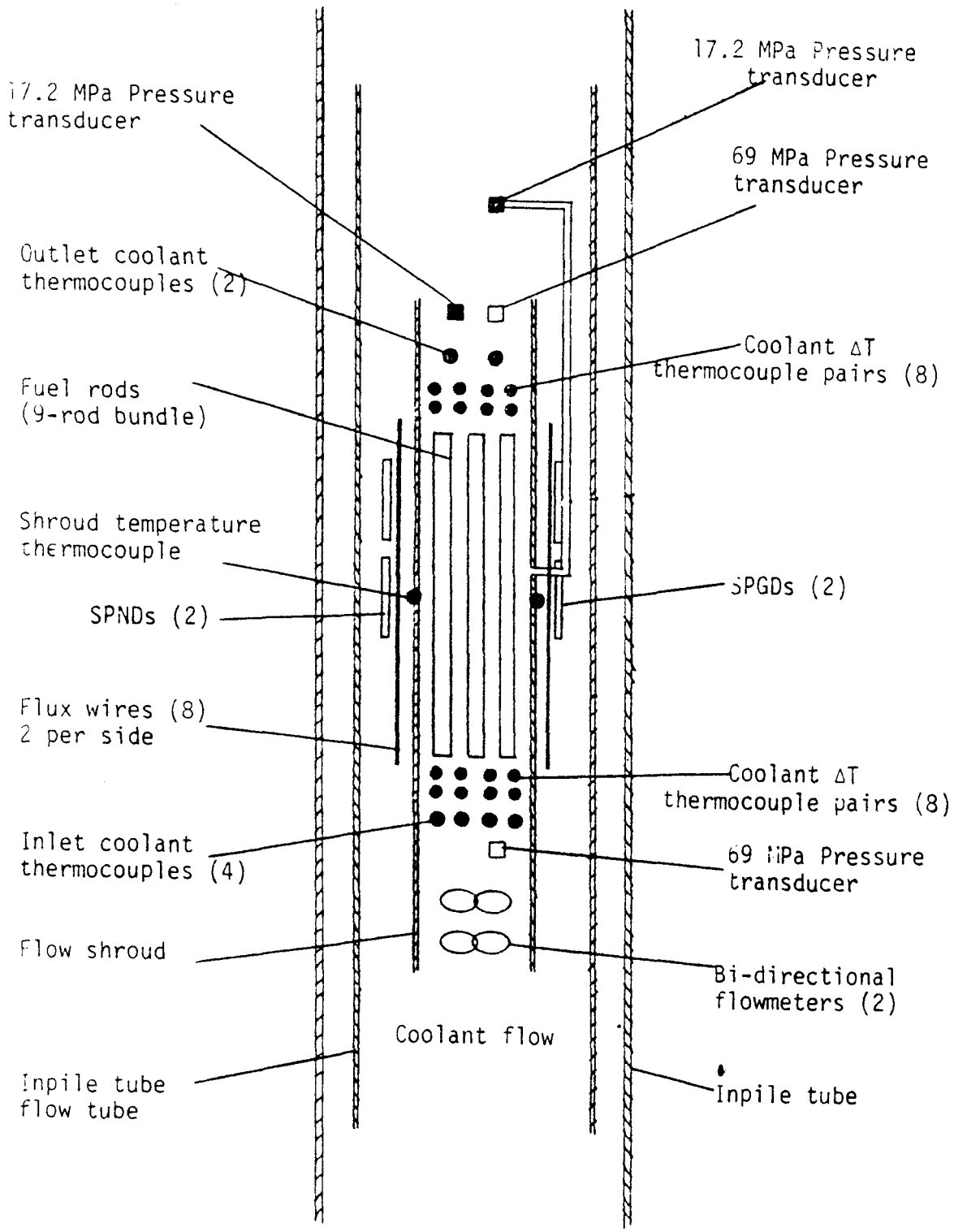


Figure 2. Test train instrumentation.

5. In-pile tube system pressure

6. In-pile tube "ΔP"

7. Loop flow rate

8. Loop fission product detection system

9. Core fuel rod linear variable differential transformers (LVDTs) (3)

10. Reactor vessel strain gauges (6)

11. Loop pressure transducers (6)

12. Ashcroft loop pressure gauge

13. Core pressure transducers (3)

In addition, four (0.51% cobalt-99.49% aluminum) flux wires were installed in the reflector and fuel regions of the core for the power calibration and preconditioning, and four 100% cobalt flux wires were installed before the power burst.

# 3. TEST CONDUCT

Test RIA 1-4 was comprised of a pre-power calibration heatup phase, a power calibration and preconditioning phase, a shutdown for fuel rod and flux wire replacement, a second heatup prior to the power burst, coolant flow measurements, the power burst and flow measurements after the power burst. Prior to each test phase and interspersed throughout the heatup phases, instrument status checks were made to detect any anomalous instrument behavior and to establish zero readings for the instruments. Several revisions were made to the Test RIA 1-4 Experiment Operating Specification[2]. These revisions are described in Document Revision Request forms. The operational phases of the test are reviewed sequentially below.

## 3.1 Pre-Power Calibration Heatup Phase

The pre-power calibration heatup phase brought the test loop to the specified coolant conditions for performing the power calibration and preconditioning; 538 K, 5.36 l/s, and 6.45 MPa.

## 3.2 Power Calibration and Preconditioning Phase

The Test RIA 1-4 power calibration and test rod fuel preconditioning were performed concurrently. The objective of the power calibration portion was to intercalibrate the thermal-hydraulically determined fuel rod power with reactor neutron detecting chambers and the neutron and gamma flux detectors mounted on the test train. The objectives of the preconditioning were to build up the short-lived fission product inventory in the fuel rod and to cause further fuel relocation. The reactor core power history during the combined power calibration and preconditioning phase, as defined from the output of the NMS-4 core ionization chamber, is summarized in Table 3.

The fuel rod bundle power calibration was accomplished by measuring coolant pressure, inlet temperature, temperatures rise from the inlet to

TABLE 3. POWER CALIBRATION AND PRECONDITIONING PHASE OPERATION

| Time Duration (minutes) | Reactor Power (MW) | Total Bundle Power (kW) |
|---|---|---|
| -- | 0 | -- |
| 22 | 0 to 100 kW | -- |
| 13 | 100 kW to 6.9 | -- |
| 10 | 6.9 | 66.6 |
| 10 | 6.9 to 100 kW | -- |
| 25 | 100 kW to 13.8 | -- |
| 10 | 13.8 | 124.2 |
| 8 | 13.8 to 100 kW | -- |
| 22 | 100 kW to 21 | -- |
| 16 | 21 | 179.8 |
| 15 | 21 to 100 kW | -- |
| 37 | 100 kW to 27 | -- |
| 13 | 27 | 221.0 |
| 13 | 27 to 100 kW | -- |
| 19 | 100 kW to 3.5 | -- |
| 8 | 3.5 | 35.7 |
| 5 | 3.5 to 100 kW | -- |
| 12 | 100 kW to 10.4 | -- |
| 10 | 10.4 | 97.2 |
| 6 | 10.4 to 100 kW | -- |
| 42 | 100 kW to 17.4 | -- |
| 10 | 17.4 | 152.0 |
| 19 | 17.4 to 100 kW | -- |
| 28 | 100 kW to 24.3 | -- |
| 11 | 24.3 | 203.3 |
| 11 | 24.3 to 100 kW | -- |
| 13 | 100 kW to 6.9 | -- |
| 13 | 6.9 | 66.8 |
| 6 | 6.9 to 100 kW | -- |
| 25 | 100 kW to 13.8 | -- |
| 11 | 13.8 | 124.0 |
| 9 | 13.8 to 100 kW | -- |
| 19 | 100 kW to 21 | -- |
| 10 | 21 | 177.8 |
| 11 | 21 to 100 kW | -- |
| 37 | 100 kW to 27 | -- |
| 10 | 27 | 220.0 |
| 2 | 27 to 0 | -- |

the outlet of the bundle, and coolant flow rate through the bundle at the measured power levels indicated in Table 4. Since the thermal-hydraulic measurements were for the nine-rod bundle, reactor physics calculated, relative rod power peaking factors of 0.88, 0.97, and 1.06 for the center, side rods, and corner fuel rods, respectively were used to determine individual fuel rod powers. An axial peak to average neutron flux ratio of 1.36 was used to calculate fuel rod peak powers. Figures 3, 4, and 5, show the figures of merit (ratio of corner rod peak power to reactor power) versus the reactor control rod position for core power chambers TR-1, TR-2, and EV-1. A regression fit of the data to a second order equation is also shown on the plots. The average of the three figure of merit values together with FRAP-T pre-test calculations were used to determine the reactor period required to obtain the desired peak fuel enthalpy of 280 cal/g $UO_2$ for the corner rods. The average figure-of-merit from the three power chambers was 1.66 kW/m per MW at the control rod position selected for the burst (0.61976 m). Reactor physics calculations had predicted a figure-of-merit of 1.54 kW/m per MW for the corner rod or about 7% lower than that measured.

### 3.3 Flux Wire and Fuel Rod Replacement

Following the completion of the power calibration and preconditioning phase, the test loop was cooled to ambient conditions and depressurized. The test train was removed from the IPT and the eight flux wires mounted on the outer surface of the flow shroud were replaced with 100% cobalt flux wires. Rod 801-2 was replaced with Rod 801-10 to permit post-test radio-chemical analysis of a fuel rod exposed only to the power burst. A radio-chemical analysis of Rod 801-2 will also be made to calibrate the flux wires located on the flow shroud and in the core during the power calibration and preconditioning phase.

### 3.4 Pre-Power Burst Heatup Phase

During the pre-power burst heatup phase test coolant conditions were established at 538 K, 6.45 MPa, and 0.766 l/s. A final evaluation of the instrument readings was made and the required adjustments were performed.

TABLE 4. SUMMARY OF TEST RIA 1-4 POWER CALIBRATION DATA

| Corner Fuel Rods Peak Power (kW/m) | Side Fuel Rods Peak Power (kW/m) | Center Fuel Rod Peak Power (kW/m) | Core Power From TR-1 Chamber (MW) | Core Power From TR-2 Chamber (MW) | Core Power From EV-1 Chamber (MW) |
|---|---|---|---|---|---|
| 11.7 | 10.7 | 9.7 | 6.8 | 6.7 | 6.9 |
| 21.8 | 19.9 | 18.1 | 13.3 | 13.4 | 13.7 |
| 31.5 | 28.8 | 26.1 | 20.2 | 20.2 | 20.8 |
| 38.7 | 35.4 | 32.2 | 25.6 | 25.6 | 26.2 |
| 6.2 | 5.7 | 5.2 | 3.4 | 3.5 | 3.3 |
| 17.0 | 15.5 | 14.1 | 10.0 | 10.2 | 10.0 |
| 26.6 | 24.4 | 22.1 | 16.4 | 16.7 | 16.7 |
| 35.6 | 32.6 | 29.6 | 23.2 | 23.3 | 23.7 |
| 11.7 | 10.7 | 9.7 | 6.6 | 6.9 | 6.5 |
| 21.7 | 19.9 | 18.0 | 13.2 | 13.4 | 13.2 |
| 31.1 | 28.5 | 25.8 | 20.0 | 20.0 | 20.3 |
| 38.5 | 35.3 | 32.0 | 25.7 | 25.6 | 26.4 |

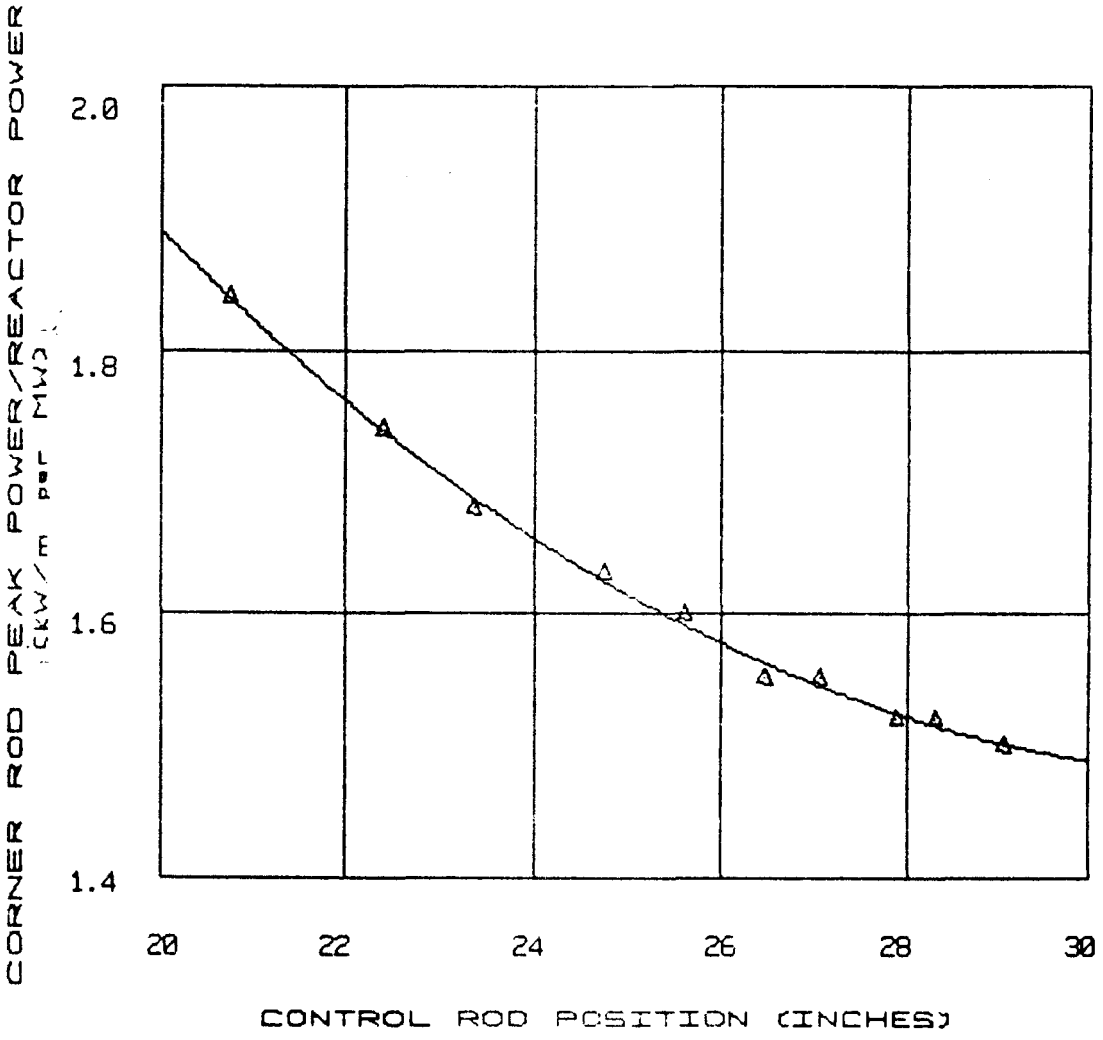


Figure 3. Ratio of corner rod peak power to reactor power as indicated by core chamber TR-1 as a function of control rod position.

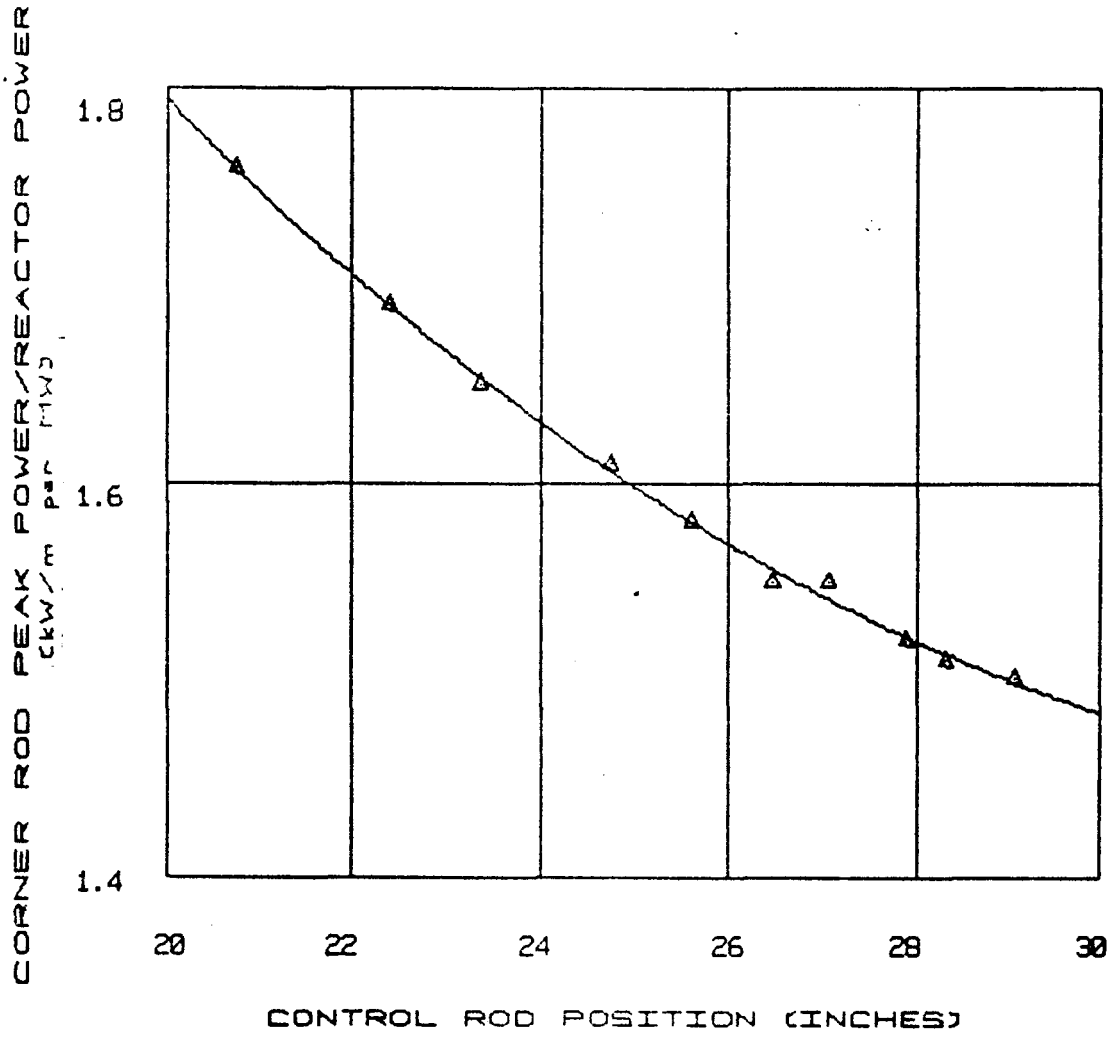


Figure 4. Ratio of corner rod peak power to reactor power as indicated by core chamber TR-2 as a function of control rod position.

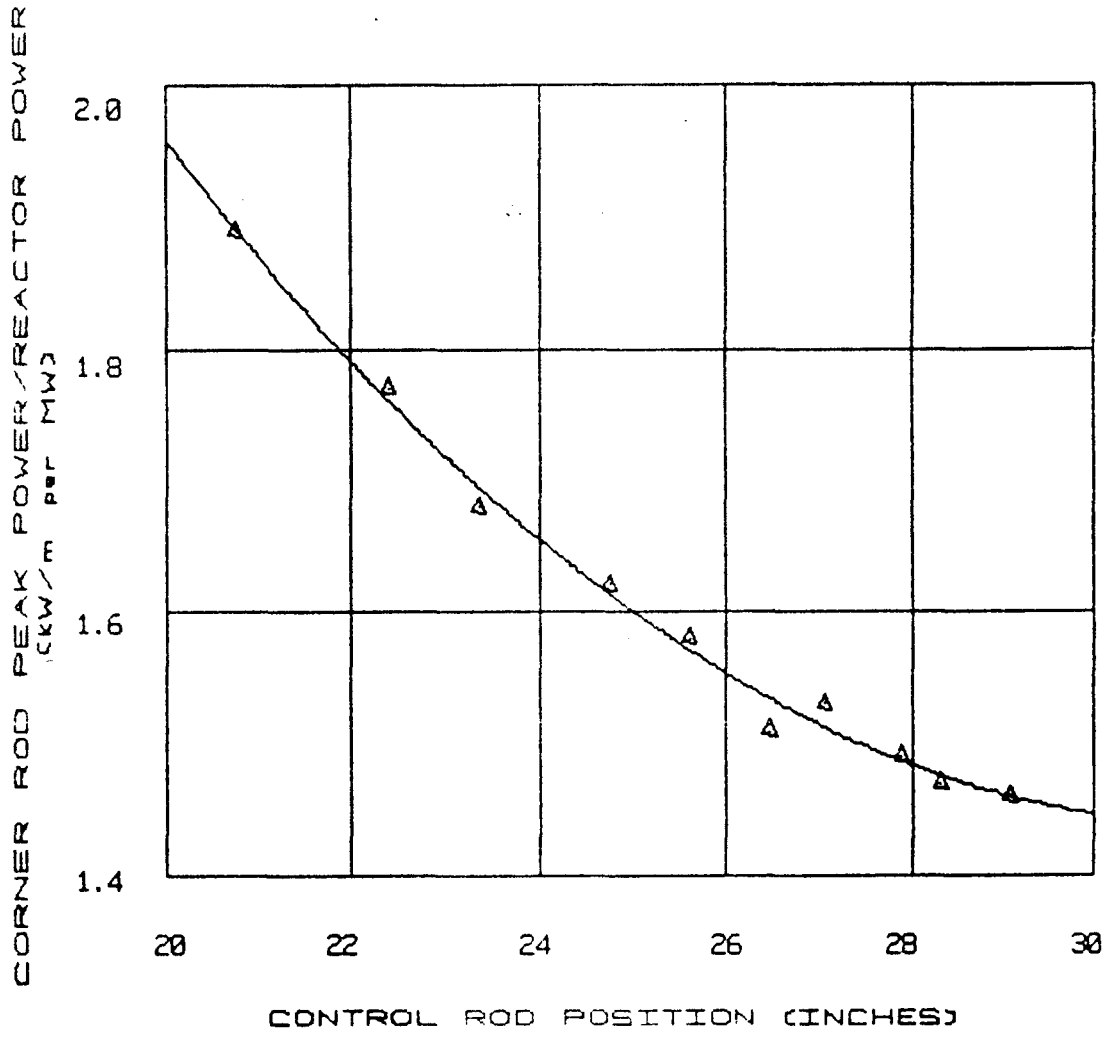


Figure 5. Ratio of corner rod peak power to reactor power as indicated by core chamber EV-1 as a function of control rod position.

Measurements of the coolant flow thorugh the shroud surrounding the fuel rod bundle and the flow bypassing the shroud were made for comparison with similar measurements after the power burst was completed. The valves on the IPT bypass line were closed for these measurements. The valves on the IPT bypass line were opened for the power burst in order to decrease the loop and shroud flow fluctuations.

## 3.5 Power Burst

The procedure to initiate the power burst is detailed below.

1. The control rods were withdrawn from their scram positions until a reactor transient period of about 10 s was achieved. The reactor power was then increased until two reactor console panel lights indicated the plant protection system was operating correctly. Immediately following verification that the plant protection system was operating, the control rods were inserted until the reactor was subcritical.

2. The control rods were then slowly withdrawn until criticality was achieved at a power of about 100 W, and the low power critical position of the control rods determined.

3. The transient rods were inserted into the core to a calculated position worth a negative reactivity equivalent to the reactivity insertion required for the power burst.

4. The control rods were then adjusted to the withdrawal position corresponding to the calculated increment for the desired reactivity insertion. The control rod withdrawal increment was checked with the transient rod insertion increment to ensure that a gross error in the control rod increment had not been made.

5. The transient rods were fully inserted into the core, leaving the control rods in a position corresponding to a calculated reactivity increment (above low-power critical) that was equivalent to the reactivity insertion desired.

6. The power burst was initiated by ejecting the four transient rods at a velocity of about 9.5 m/s. The burst was self-terminating because of the inherent Doppler reactivity feedback in the PBF. The feedback is capable of terminating power bursts without primary dependence on mechanical systems.

7. All eight control rods were then completely inserted into the driver core to provide mechanical shutdown of the reactor.

A single power burst having a reactor period of about 2.8 ms and a peak power of about 37,000 MW was performed for Test RIA 1-4. The reactor power during the burst is illustrated by the response of the EV-1 core power chamber shown in Figure 6. The energy deposition data for the power burst are summarized in Table 5. Based on the average of the data, a total fuel energy of 354 cal/g $UO_2$ was deposited in the corner fuel rods, 325 cal/g $UO_2$ in the side fuel rods, and 297 cal/g $UO_2$ in the center rod. These total fuel energy values include 15 cal/g $UO_2$ equivalent to the initial zero power temperature of 538 K. The energy deposited at the time of control rod scram were: 277 cal/g for the corner rods, 254 cal/g for the side rods, and 230 cal/g for the center rod.

A post-test FRAP-T5 calculation was made to determine the peak fuel enthalpy of the corner rods using the average energy deposition from the four core chambers and one of the SPNDs. The data used in the calculation was the same as that used in the pretest RIA 1-4 experiment prediction report with the exception of the fuel rod power history. The fuel rod power hsitory shape was obtained from the EV-1 core chamber response out to reactor scram which occurred about 30 ms past the time of peak power. The fuel rod power burst shape was nomalized to produce a fuel rod energy deposition of 277 cal/g $UO_2$ (292 cal/g $UO_2$ including initial fuel temperature) at the axial peak location. The results of the calculation indicate that a radially averaged peak fuel enthalpy of 281 cal/g $UO_2$ was obtained at the axial peak in the corner rod about 18 ms after the time of peak power. The peak local fuel enthalpy was about 338 cal/g $UO_2$ for the corner rod.

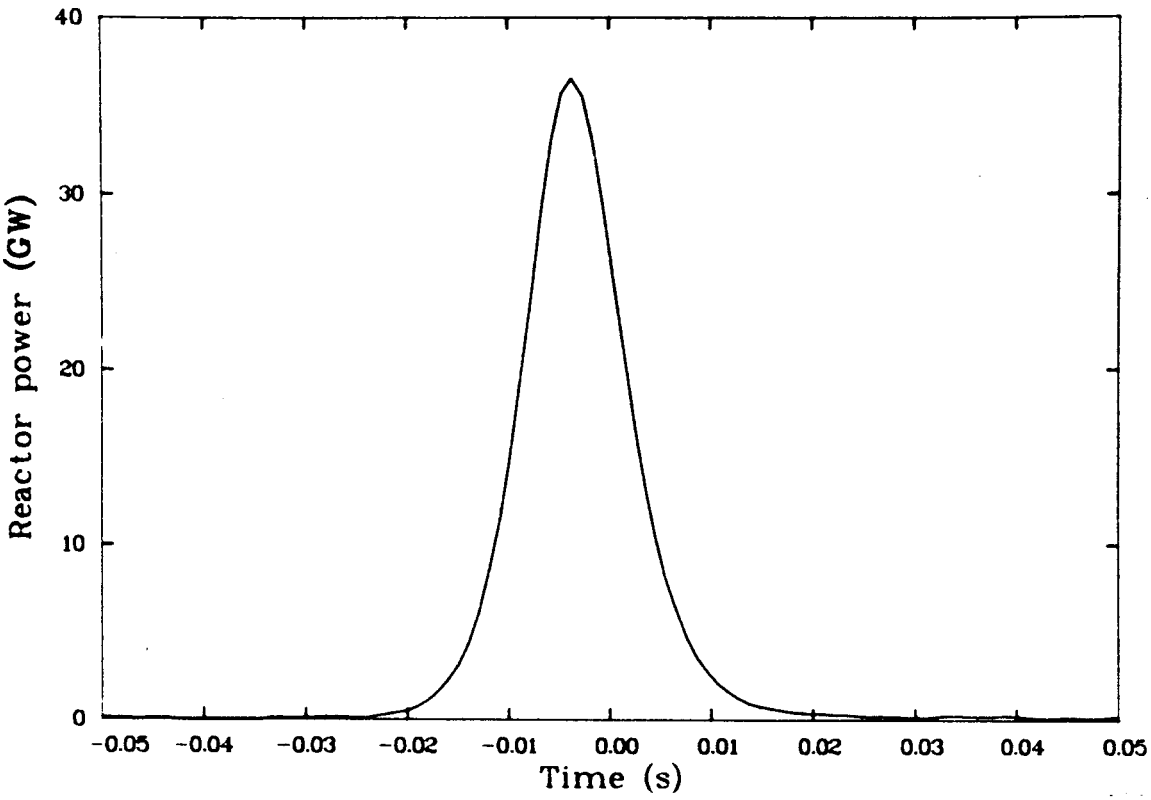


Figure 6. Reactor power during the Test RIA 1-4 power burst as indicated by core chamber EV-1.

TABLE 5. TEST RIA 1-4 FUEL ENERGY DATA SUMMARY

| Neutron Detecting Chamber Designation | Corner Rod Energy Deposited at Scram (cal/g UO2) | Corner Rod Total Energy[a] At Scram (cal/g UO2) | Corner Rod Total Energy[a] (cal/g UO2) | Corner Rod Peak Fuel Enthalpy (cal/g UO2) |
|---|---|---|---|---|
| TR-1 | 266 | 281 | 340 | |
| TR-2 | 263 | 278 | 336 | |
| EV-1 | 292 | 307 | 372 | |
| EV-2 | 288 | 303 | 367 | |
| SPND-0 01 | 274 | 290 | 350 | |
| | 277 Average | 292 Average | 353 Average | 281 |
| | 13 (1J) | 13 (1J) | 16 (1J) | |

The fuel energy data derived from the other neutron and two gamma flux detectors located on the flow shroud were very low, ($\sim$150 cal/g $UO_2$) and were therefore rejected. Further investigation of this data will be required.

Final determination of the fuel energy deposited during the RIA 1-4 power burst must await completion of burnup analysis of the fuel rods, neutron fluence measurements from the cobalt flux wires and data qualification of the on-line data.

Following the power burst, the fission product detection system indicated that fuel rod failure had occurred. About 20 s after the power burst, the coolant flow thorugh the shroud rapidly decreased by about 50% indicating partial flow blockage. The maximum measured cladding surface temperature was 1625 K on the corner rod. A coolant pressure pulse of 1.9 MPa above the system pressure of 6.45 MPa was indicated by the pressure transducer connected by tubing to the flow shroud. It is believed that all nine fuel rods failed as predicted, but hot cell examination will be required to confirm the extent of fuel rod failure.

## 4. TEST RESULTS

The response of the fuel rod and shroud instruments during Test RIA 1-4 along with a brief discussion of the fuel rod behavior are presented in this section. The FRAP-T comparisons with cladding surface temperature measurements were obtained from the FRAP-T5 calculations described in the Test RIA 1-4 Experiment Prediction Report.[4] The data have not been qualified so conclusions about the fuel rod response are preliminary. All times quoted are relative to the time of peak power.

### 4.1 Cladding Surface Temperature

Three rods, 804-1, 804-5, 804-6, were instrumented with two thermocouples each. The thermocouples located at the 0.79 m location on Rods 1 and 5 failed during the test. Figures 7 and 8 show the 0.59 m

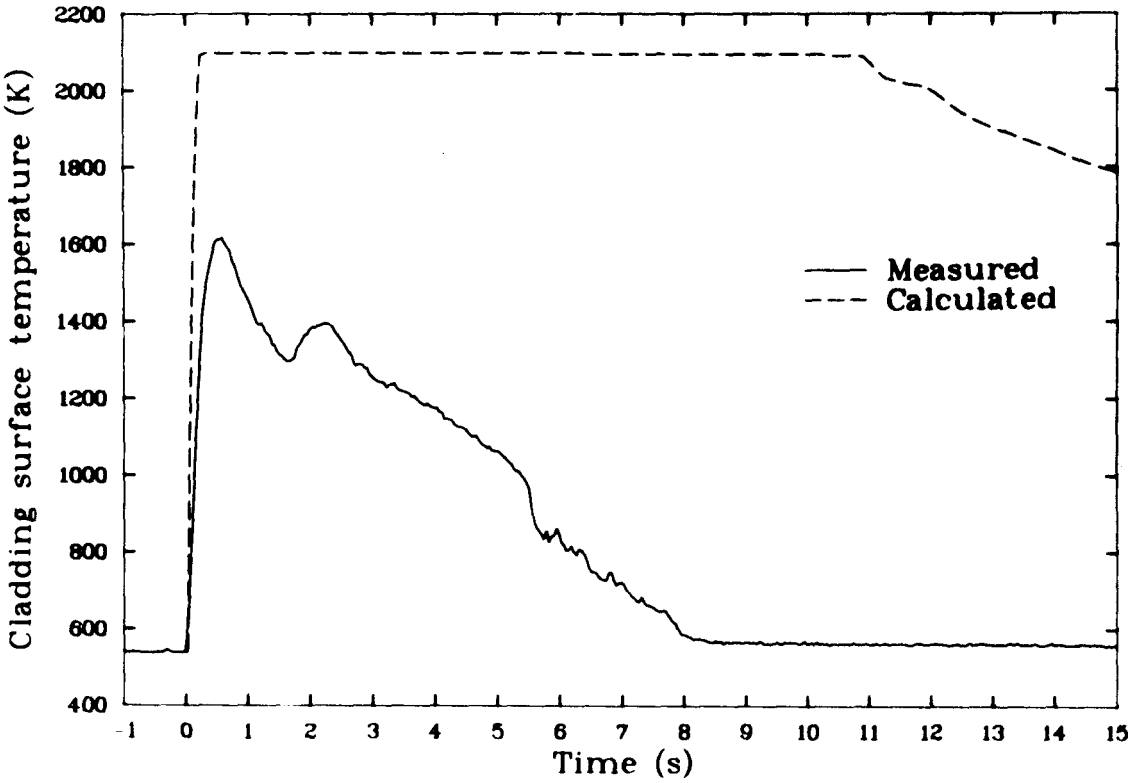


Figure 7. Response of the cladding thermocouple at 0.59 m - 315° on the center rod (804-1) on the calculated cladding temperature following the Test RIA 1-4 power burst.

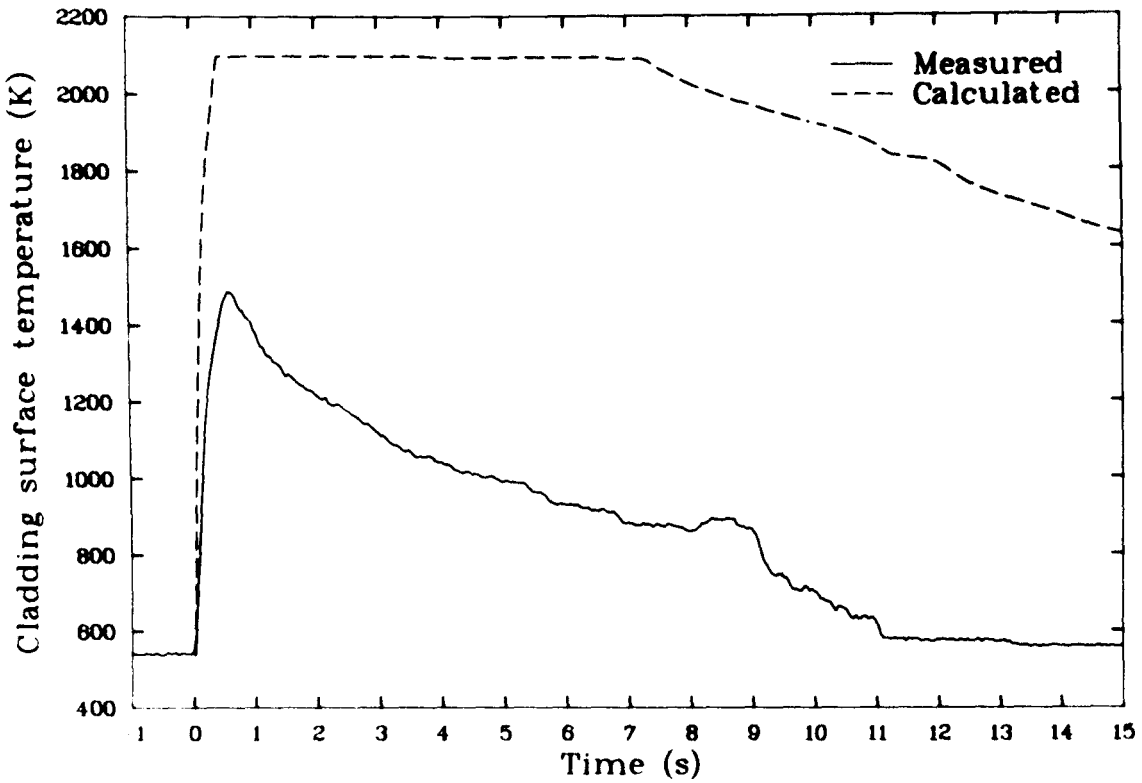


Figure 8. Response of the cladding thermocouple at 0.59 m - 315° on center rod (804-5) and the calculated cladding temperature following the Test RIA 1-4 power burst.

thermocouple response for the corner (804-1) and center (804-5) rods, respectively, along with the FRAP-T calculated cladding surface temperature. Figure 7 indicates that the 0.59 m thermocouple on the corner rod measured a peak cladding surface temperature of 1625 K at 0.57 s after peak power as compared to a calculated temperature of 2100 K (zircaloy melting temperature) from 0.33 to 59 s. The thermocouple response also indicated that the time in film boiling was approximately 5.5 s which was much shorter than the calculated film boiling time of 29 s. The lower measured temperatures and shorter film boiling times have also been observed in previous RIA tests. Post-test examinations have indicated that the indicated cladding temperatures may be low by 100-200 K. Results from the PCM-5 9-Rod bundle test showed that the grid spacers effectively stop the film boiling zone propagation. Since the 0.59 m thermocouple was only 1 cm below the 0.625 grid spacer, the short film boiling time as measured by the thermocouple may be an indication of a grid spacer effect on film boiling. Between 5.5 and 8.0 s, the thermocouple response shows a gradual decrease with temperature fluctuations instead of the sharp temperature drop usually seen when the cladding quenches. The observed thermocouple response between 5.5 and 8.0 s may be an indication of a return to transition boiling followed by a nucleate boiling heat transfer in a temperature controlled system.

The response of the 0.59 m thermocouple on the center rod is shown in Figure 8. The maximum indicated temperature is about 1500 K. The film boiling-transition boiling-nucleate boiling transition is indicated in Figure 8 between 9 and 11 s. The observed 9 s film boiling time as opposed to a calculated film boiling time of >29 s may be due to some grid spacer effect. The lower than calculated temperatures is probably due to a thermocouple fin effect and/or movement of the thermocouple away from the cladding during the burst.

Figures 9 and 10 present comparison plots of the calculated and measured cladding surface temperatures at the 0.60 and 0.79 m location on the side rod (804-6). The plots are very similar to Figures 7 and 8 in that both figures show measured temperatures lower than that calculated by

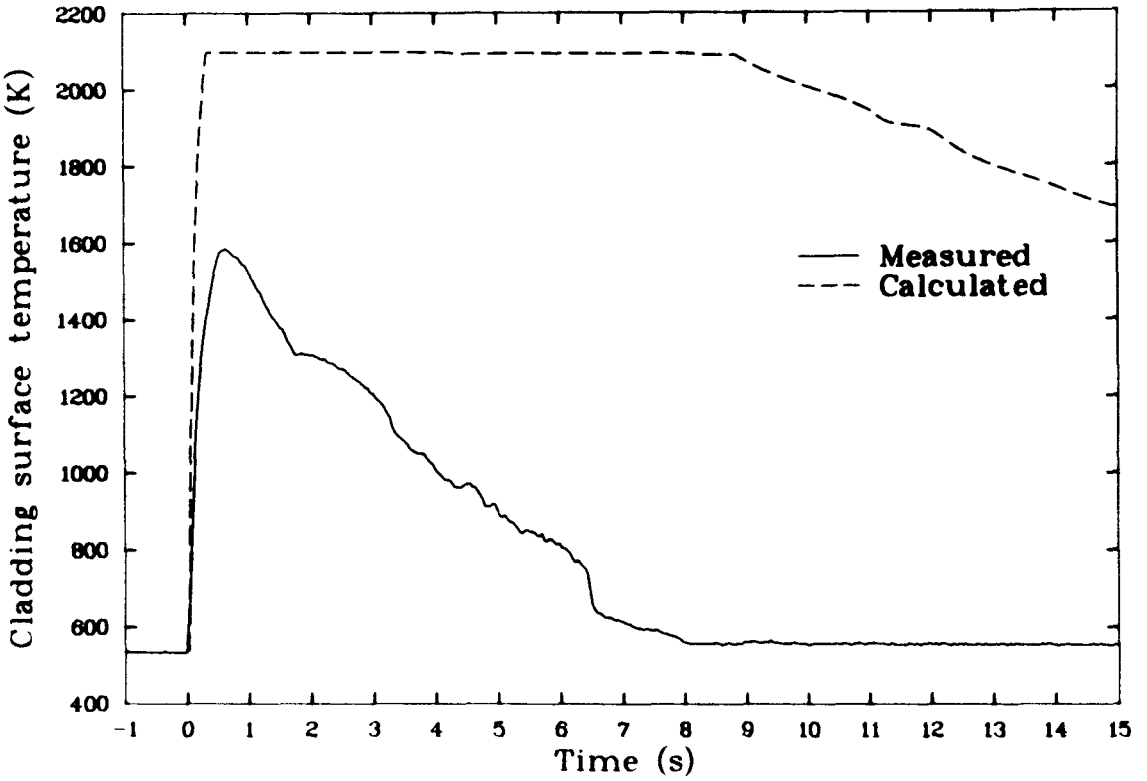


Figure 9. Response of the cladding thermocouple at 0.60 m - 135° on side rod (804-6) and the calculated cladding temperature following the Test RIA 1-4 power burst.

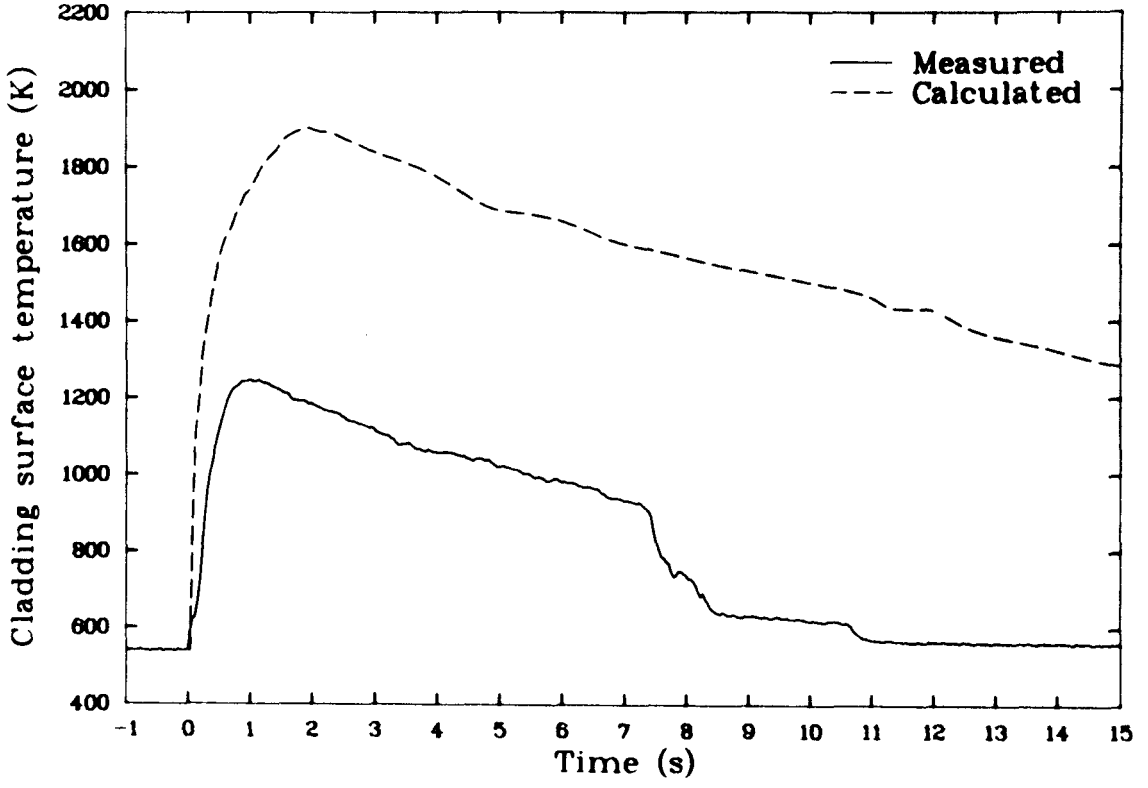


Figure 10. Response of the cladding thermocouple at 0.79 m - 315° on side rod (804-6) and the calculated cladding temperature following the Test RIA 1-4 power burst.

FRAP-T5 and measured film boiling times shorter than that calculated by FRAP-T5. Indications of the film-transition-nucleate boiling process is also seen in Figure 9 between 7.5 and 11.0 s and in Figure 10 between 6 and 8 s. Figure 10 shows a change in the rate of temperature decrease at 4 s and the other thermocouples also showed a change in the temperature slope between 1 and 4 s. This was probably due to the rapid pressure drop that was measured between 1 and 4 s and the resulting decrease in the saturation temperature of the system. As the saturation temperatures dropped the coolant was able to cool the rods at a faster rate becasue extra energy was required for the coolant heat of vaporization.

## 4.2 Shroud Pressure

Figure 11 is the shroud pressure transducer response from -5 to 30 s and shows the pressure pulse and subsequent decrease that occurred between 0.5 and 4.0 s. Figure 12 shows the pressure transducer response from -0.5 to 1.0 s. The large pressure pulse near the time of peak power was probably due to the direct $\gamma$ and neutron heating of the coolant during the burst. Figure 12 shows that following the initial pressure pulse, a series of smaller pulses occurred between 0.1 and 0.4 s. These pulses were fairly regular occurring at intervals of 50-95 ms and were probably due to a ringing effect caused by the initial pressure pulse and reflections of that pulse in the in-pile tube.

## 4.3 Outlet Coolant Temperature

Figure 13 shows the outlet thermocouple response during the test along with the calculated saturation temperature obtained from the pressure response shown in Figure 10. Figure 12 indicates that the outlet coolant was above the saturation temperature until about 22 s.

## 4.4 Shroud Temperature

Figures 14 and 15 show the two shroud thermocouple responses from -1 to 15 s. The thermocouples were placed on the outside of the shroud on

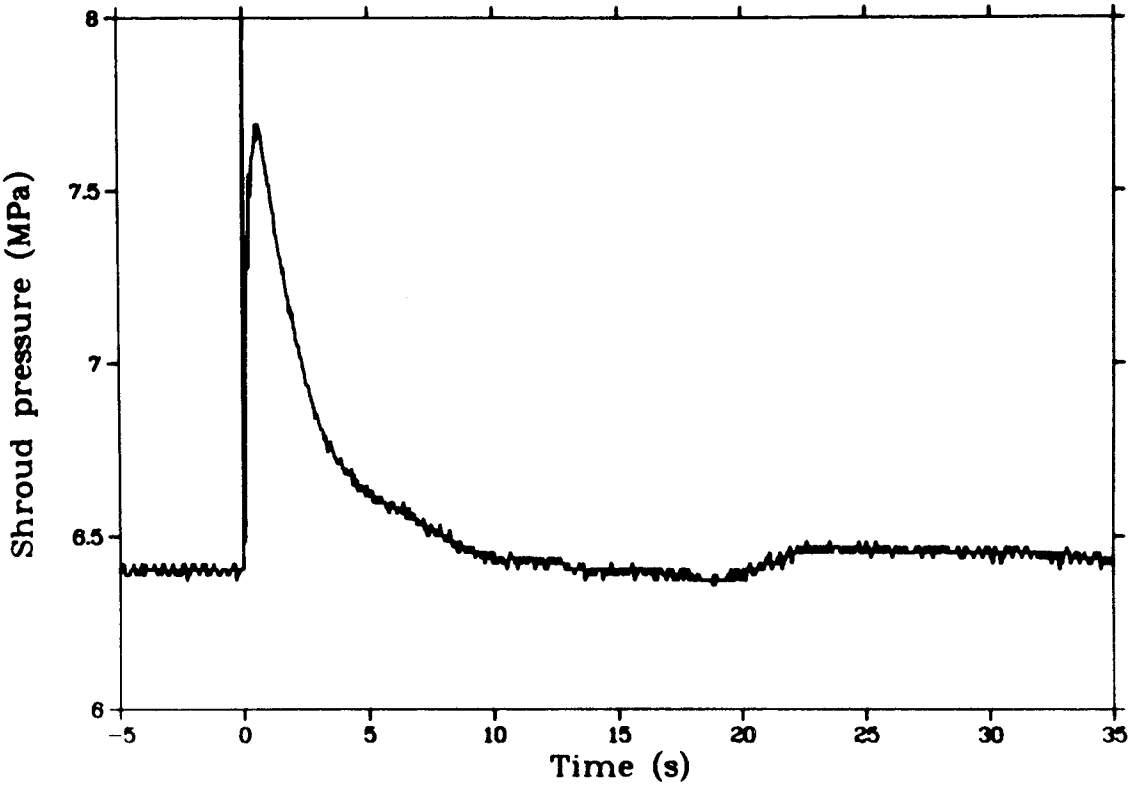


Figure 11. Response of the 17-MPa EG&G shroud pressure transducer to the source pressure during the Test RIA 1-4 power burst (-5 to 35 s).

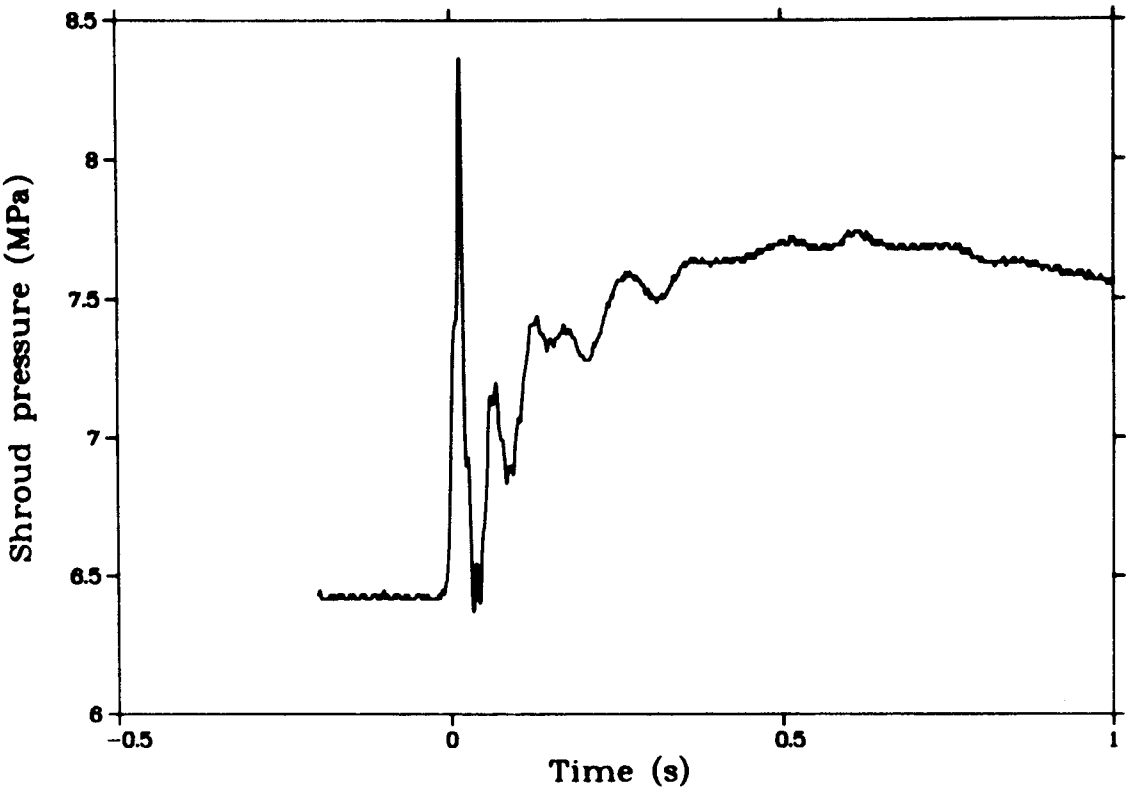


Figure 12. Response of the 17-MPa EG&G shroud pressure transducer to the source pressure during the Test RIA 1-4 power burst (-0.5 to 1.0 s).

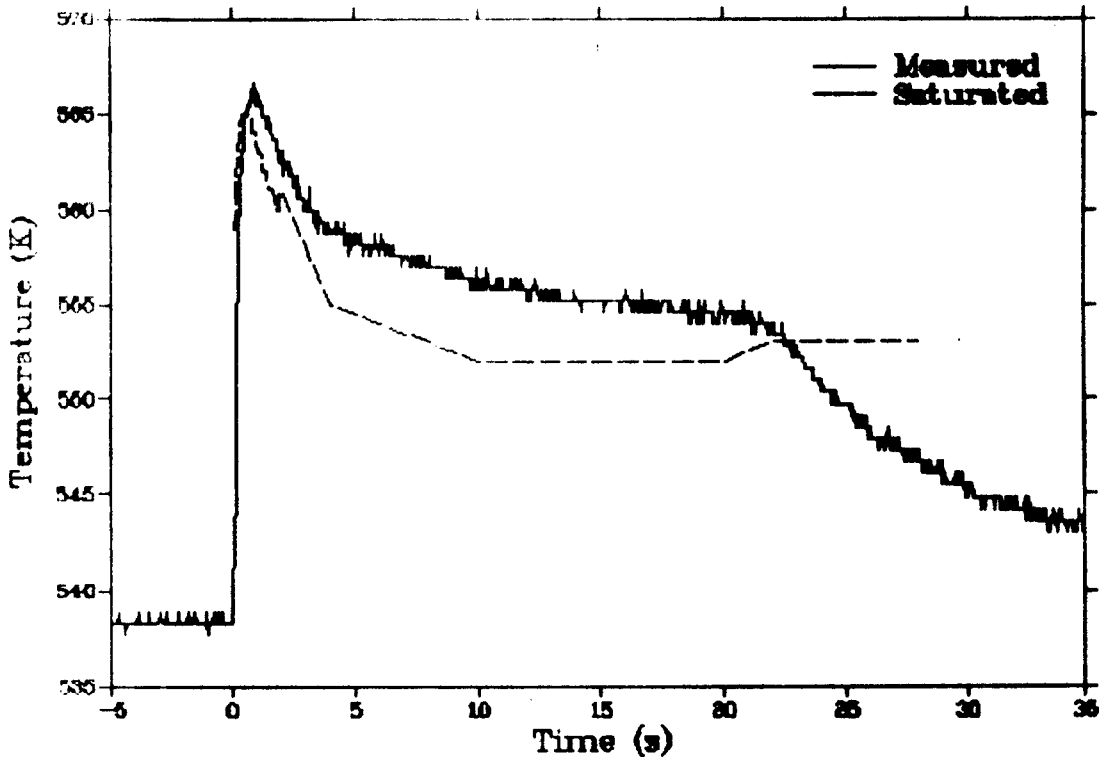


Figure 13. Response of the outlet coolant thermocouple and calculated water saturation temperature during the Test RIA 1-4 power burst.

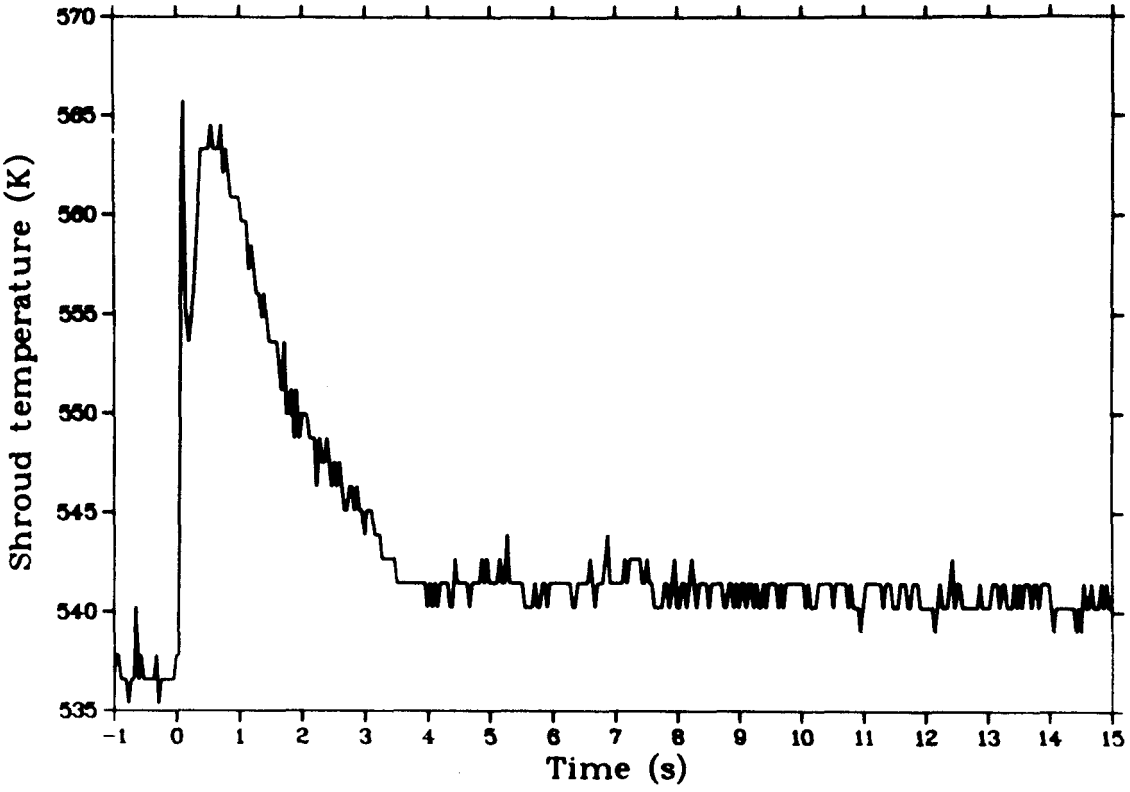


Figure 14. Response of the shroud thermocouple (0° orientation) during the Test RIA 1-4 power burst.

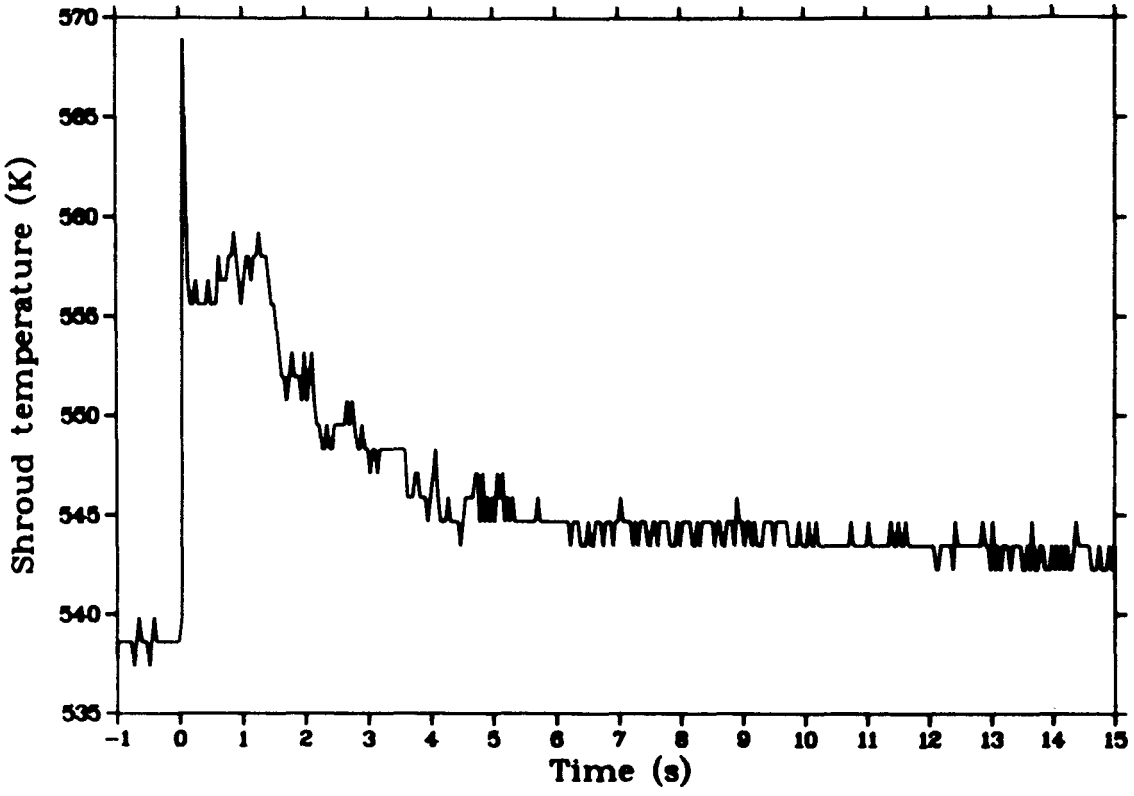


Figure 15. Response of the shroud thermocouple (180° orientation) during the Test RIA 1-4 power burst.

opposite faces at the axial peak location (0° and 180°). The initial temperature spike seen in both figures was probably due to the direct Y and prompt neutron heating of the shroud wall and coolant during the burst. Figure 14 shows a second temperature peak of 564 K at 1 s followed by fairly smooth decrease from 1 to 3.5 s whereas Figure 15 does not show a pronounced second peak but does show smaller temperature fluctuations. The temperature fluctuations shown in Figure 15 are probably due to slugs of coolant rewetting and drying out the inner shroud wall. The temperature measured in Figure 14 indicates that the inside wall was not wetted since the peak temperature measured by the thermocouple was above the saturation temperature of the coolant inside the shroud.

## 4.5 Inlet Flowmeter Response

The inlet flowmeter response during Test RIA 1-4 a from -20 s to 180 s and from -1 s to 2 s are shown in Figures 16 and 17, respectively. Both flowmeters measured flow reversal (-1.6 l/s) during the burst followed by a flow stagnation for about 0.5 s. The flow gradually increased to the pre burst flow rate between 1 and 8 s. The gradual flow increase corresponds to the decrease in shroud pressure that occurred during the same time interval. At 20 s after the power burst both shroud flow measurements decreased to about 50% of the pre-power burst flow rate indicating partial flow blockage. The flow decrease corresponds to the slight shroud pressure increase that occurred at 20 s (Figure 11).

## 4.6 Bundle Thermal-Hydraulic Response

A composite plot of the shroud coolant outlet temperature, pressure and inlet flow rate is shown in Figure 18. A sharp increase of coolant pressure in the test bundle up to ~8.4 MPa, occurred due to the rapid overheating of the water coolant by gamma radiation from the PBF core during the power burst. The cladding surface temperature was not high enough to initiate film boiling. A similar pressurization of the coolant may have occurred in the bypass flow tube. The pressurized liquid within

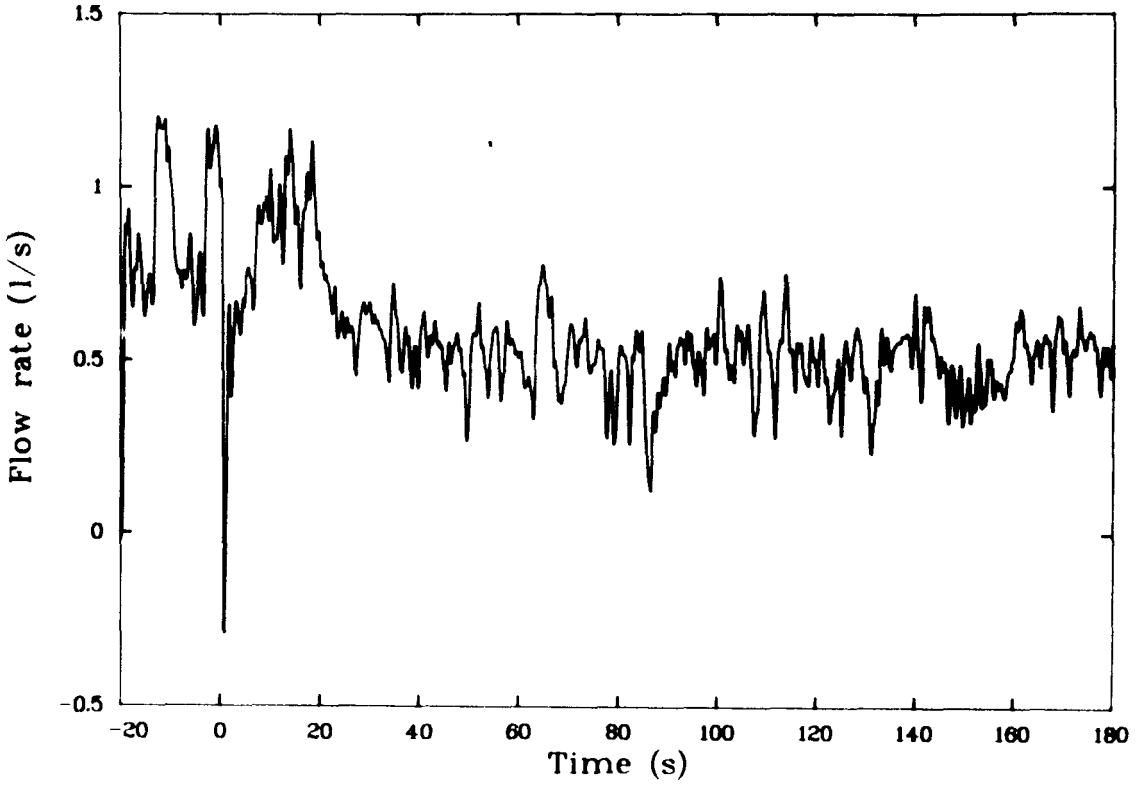


Figure 16. Response of the shroud inlet flowmeter during the Test RIA 1-4 power burst (-20 to 180 s).

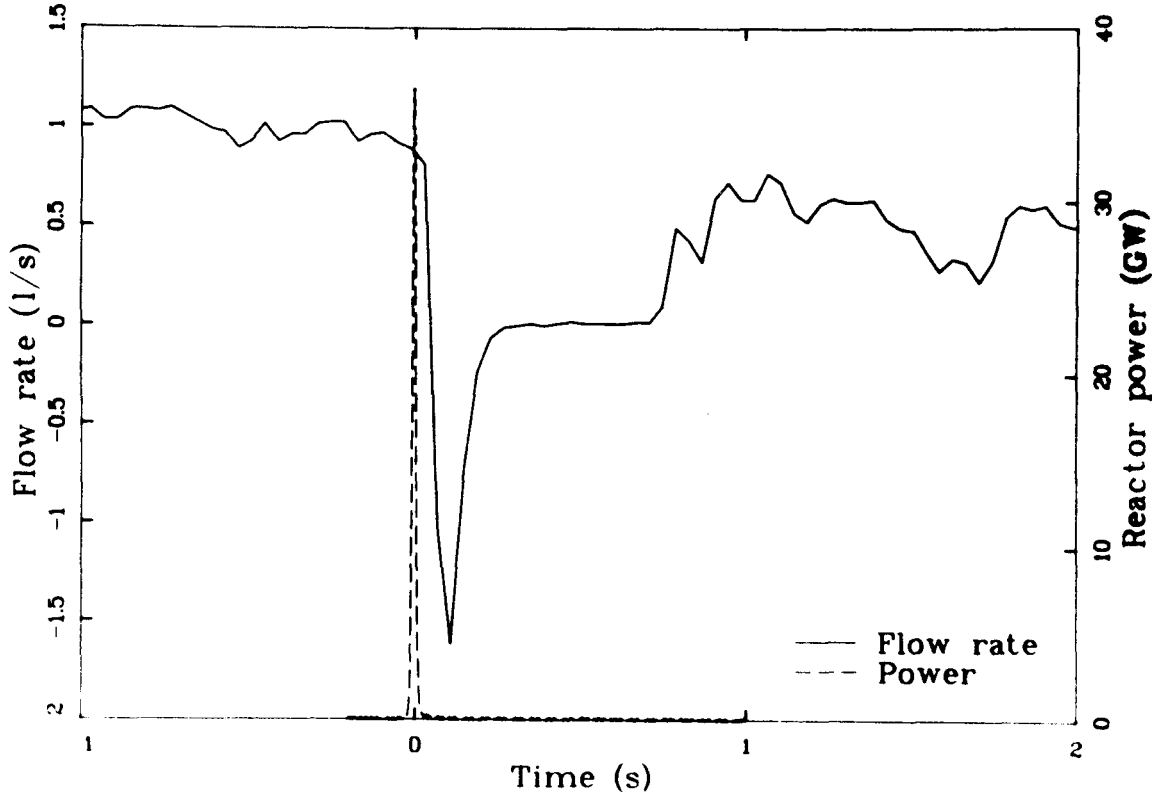


Figure 17. Response of the shroud inlet flowmeter and reactor power time history during the Test RIA 1-4 power burst (-1 to 2 s).

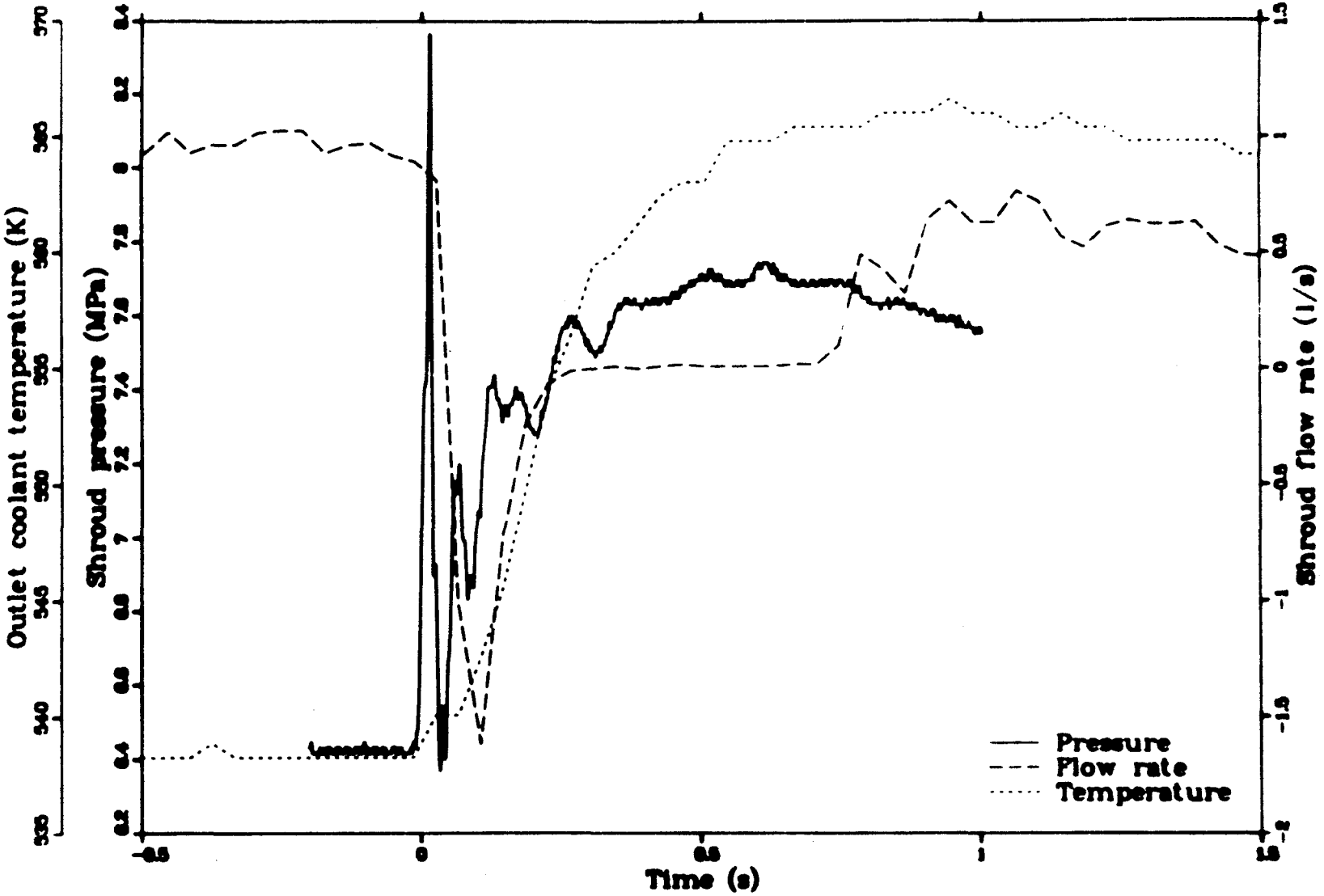


Figure 18. Composite plot of shroud outlet coolant temperature, shroud pressure, and shroud inlet flow rate during Test RIA 1-4 power burst.

the shroud expands against the system producing a flow excursion at both ends of the test bundle as indicated by the turbine flow meters installed at the inlet of the shroud.

The flow excursion out of the shroud was fast at the beginning and slowed down as the pressure in the shroud decreased to the loop pressure ($\sim$6.45 MPa). The integration of the flow trace at the inlet of the shroud indicates that about 150 $cm^3$ of the coolant (about 25% of the coolant over the lower half of the active fuel rods) was expelled from the shroud inlet. This indicates that about 25% of the bundle could have been voided by the coolant excursion from both ends of the bundle.

The heat energy transferred from the test rods to the steam void formed within the shroud by water flashing during the flow excursion process increased the steam pressure in the bundle and inhibited the collapse of the bubble. The coolant flow completely stopped for about 0.5 s about 0.2 s after the power burst. This flow stagnation has not been observed in previous separately shrouded single fuel rod RIA tests.

The steam bubble in the fuel bundle started to cool off and collapse when the heat flux from the rods was less than that being transferred out by conduction through the bundle wall and by coolant entrapment at the upper and lower interfaces of the bubble. As the pressure in the bundle decreased, upward flow through the shroud was restored. The partial collapse of the steam bubble increased the coolant temperature at the exit of the bundle slightly above the saturation temperature of the coolant ($\sim$552 K). At this time the test rods were in stable film boiling as indicated by the cladding surface thermocouples. In summary, the scenario of events in the RIA 1-4 can be briefed as:

1. Rapid coolant pressurization by gamma heating

2. Flow Excursion

3. Voiding of the bundle

4. Void partial collapse

5. Stable film boiling on the surface of the test fuel rods

6. Quenching of the test rods by film boiling collapse.

## 5. ASSESSMENT OF FLOW BLOCKAGE

The main objective of the RIA-1-1 was to investigate the occurrence of flow blockage in the fuel bundle following the power burst. It was hypothesized that fragmented fuel particles would relocate within the flow shroud forming a rubble bed which would be fluidized by the inlet coolant flow to the bundle. Therefore, a comparison of the shroud coolant flow before and after the burst could indicate the occurrence and the extent of the flow blockage.

The coolant flow rate to the fuel bundle was measured using two bidirectional turbine flowmeters mounted in series at the inlet of the shroud. The total coolant flow to the in-pile tube (IPT) as well as the pressure drop across the IPT were measured. These flow measurements were taken about 5 hours after the power burst after the loop flow bypass line valves were closed. The bypass coolant flow within the IPT was calculated by subtracting the shroud coolant flow from the total loop flow. The measurements of the shroud coolant flow rate as a function of IPT flow rate, and consequently the coolant bypass flow rate, before and after the burst, are listed in Table 6. Since the pressure drop across the shroud is proportional to the bypass flow rate, the same bypass flow before and after the burst should indicate the same pressure gradient across the shroud. Table 7 lists the hydraulic parameters of the test fuel bundle. This was confirmed by the measurements of the pressure drop across the inpile tube and the coolant flow rates taken before and after the power burst.

A plot of the shroud inlet flow as a function of the IPT bypass flow is shown in Figure 19. This data indicates that for a given bypass flow, the shroud flow increased as a result of the power burst which is in contrast to the shroud flow reduction observed about 20 s after the power burst. Fuel washout may have occurred in the intervening 5 hours duration.

TABLE 6. FLOW MEASUREMENTS

| Shroud Inlet Flow-1 (l/s) | Shroud Inlet Flow-2 (l/s) | Average Shroud Inlet Flow (l/s) | Total Inpile Tube Flow (l/s) | Inpile Tube Bypass Flow (l/s) | Inpile Tube P (MPa) |
|---|---|---|---|---|---|
| | | Before Power Burst | | | |
| 0.12 | 0.49 | 0.49 | 6.97 | 6.48 | 0.03 |
| 1.77 | 1.79 | 1.78 | 10.26 | 8.48 | 0.05 |
| 1.28 | 1.04 | 1.16 | 5.70 | 4.54 | 0.03 |
| 5.49 | 5.58 | 5.54 | 14.17 | 8.63 | 0.35 |
| 5.09 | 5.03 | 5.08 | 14.08 | 9.02 | 0.30 |
| 4.01 | 4.02 | 4.01 | 12.59 | 8.58 | 0.20 |
| 3.06 | 3.09 | 3.08 | 11.56 | 8.49 | 0.13 |
| | | After Power Burst | | | |
| 1.30 | 1.18 | 1.24 | 4.85 | 3.60 | 0.04 |
| 1.88 | 1.90 | 1.89 | 8.57 | 6.68 | 0.06 |
| 2.09 | 2.06 | 2.05 | 9.11 | 7.06 | 0.07 |
| 2.31 | 2.33 | 2.32 | 10.10 | 7.78 | 0.09 |
| 2.82 | 2.86 | 2.84 | 11.01 | 8.17 | 0.12 |
| 2.99 | 3.02 | 3.01 | 11.36 | 8.35 | 0.14 |
| 3.35 | 3.38 | 3.37 | 11.70 | 8.34 | 0.16 |
| 3.71 | 3.74 | 3.73 | 12.33 | 8.61 | 0.20 |
| 4.01 | 4.03 | 4.02 | 12.78 | 8.76 | 0.23 |
| 4.43 | 4.45 | 4.44 | 13.15 | 8.71 | 0.28 |
| 5.01 | 4.99 | 5.00 | 13.97 | 8.97 | 0.33 |
| 5.34 | 5.29 | 5.32 | 14.45 | 9.13 | 0.37 |
| 4.08 | 4.10 | 4.09 | 12.68 | 8.59 | 0.24 |
| 2.97 | 3.01 | 2.99 | 11.39 | 8.40 | 0.14 |
| 2.06 | 2.08 | 2.07 | 10.04 | 7.97 | 0.08 |
| 1.16 | 0.69 | 0.92 | 8.52 | 7.60 | -- |

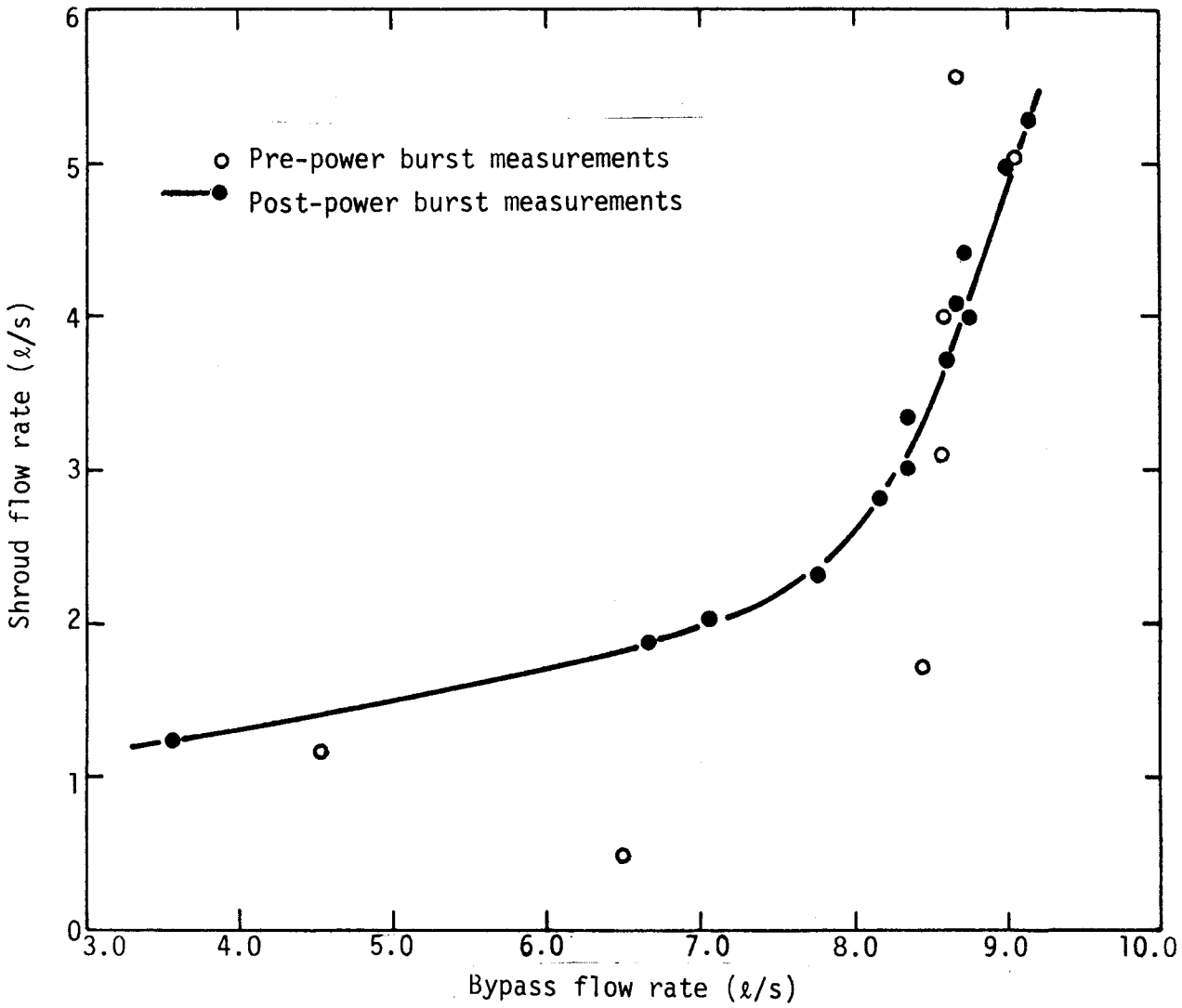


Figure 19. Measurements of shroud coolant flow rate as a function of inpile tube bypass coolant flow rate taken before and after the Test RIA 1-4 power burst.

TABLE 7. HYDRAULIC PARAMETERS OF THE RIA-1-4 FUEL BUNDLE BEFORE THE BURST

| Parameter | Value |
|---|---|
| 1. Equivalent hydraulic diameter, $D_e$ (cm) | 1.188 |
| 2. Geometrical Flow Area, $A_G$ ($cm^2$) | 13.485 |
| 3. Inlet Flow Rate during the burst, Q (l/s) | 0.766 |
| 4. Inlet flow velocity (m/s) | 0.568 |
| 5. Reynolds Number of the flow during the burst, Re | $4.934 \times 10^4$ |

As indicated in Table 7 the Reynolds number within the flow shroud prior to the burst was in the turbulent range. Therefore the pressure gradient across the bundle, $\Delta P/L$, can be given by the relation

$$\frac{\Delta P}{L} = \frac{4}{D_e} \frac{\rho_c V^2}{2} f \qquad (1)$$

where $\rho_c$, V are the coolant density and inlet velocity, respectively; f is the friction loss coefficient, given as

$$f = \frac{0.0791}{R_e^{0.25}}, \text{ for } 2.1 \times 10^3 < R_e < 10^5 \qquad (2)$$

Eliminating f between equation 1 and 2 gives;

$$\frac{\Delta P}{L} = 0.1582 \quad \frac{\rho_c^{0.75} \mu^{0.25} V^{1.75}}{D_e^{1.25}} \tag{3}$$

For $\rho_c$ = 0.786 g/cm$^3$, $\mu$(coolant viscosity) = 1.075 x $10^{-3}$ g/cm s, and $D_e$ = 1.188 cm (see Table 1); Equation 3 can be simplified as

$$\frac{\Delta P}{L} = (2.032 \times 10^{-4})\, Q^{1.75} \tag{4}$$

In Equation 4, Q is the inlet volumetric flow rate of the coolant in the shroud before the burst and ($\Delta P/L$) is the pressure gradient from the shroud inlet to the shroud outlet.

After the burst fuel fragmentation and relocation within the shroud could result in the formation of a rubble bed which can be fluidized by the coolant flow thorugh the shroud. In this case the coolant hydraulics in the fuel bundle would be entirely different than before the burst.

For flow through a fluidized bed, the characteristics of the bed are defined as follows to calculate the pressure drop across the shroud after the burst. The Reynolds number in the rubble bed $B_{Re}$ is defined as

$$B_{Re} = \frac{D_p \rho_c V_o}{\mu} \tag{5}$$

In the above equation $V_o$ is the superficial velocity of the coolant through the bed and $D_p$ is the mean particle diameter defined as:

$$D_p = \frac{6\,(1-\varepsilon)}{\alpha \phi s} \tag{6}$$

where $\varepsilon$ is the void fraction void in the particle bed, and $\alpha$ is the particle specific surface area, and $\phi_s$ is the sphericity of the debris particles. These parameters are defined in order, as follows:

a. $$\varepsilon = \frac{\text{volume of voids}}{\text{volume of bed}}$$

$$\varepsilon = \frac{\text{Flow area in the bed}}{\text{Geometrical cross-section of the bundle}}$$

$$\varepsilon = (1 - \xi) \qquad (7a)$$

where $\xi$ is the flow blockage fraction due to the formation and the fluidization of the bed. It should be noted that $\xi$ is dependent on the rubble bed characteristics as well as the fluidization conditions of the bed.

b. The specific surface area of the fuel rubbles, $\alpha$, is given as

$$\alpha = \frac{\text{surface area of the particle}}{\text{volume of the particle}} \quad , \quad = (6/\phi_s D_p) \qquad (7b)$$

c. The sphericity of the particles, $\phi_s$, is defined as

$$\phi_s = \left( \frac{\text{surface area of a sphere}}{\text{surface area of the particle}} \right) \quad \text{both of the same volume.} \qquad (7C)$$

Equation 5 can now be written in terms of the flow blockage in the bundle after the burst, as

$$B_{Re} = \frac{6 \xi \rho_c V_o}{\alpha \rho_s \mu} \qquad (8)$$

Substituting for $\rho_c$ and $\mu$ as 0.786 g/cm$^3$ and 1.075 x $10^{-3}$ g/cm s, respectively, equations (8) is simplified as

$$B_{Re} = 4.387 \times 10^3 = 4.387 \times 10^3 \quad \frac{\xi \; Q_B}{\alpha \phi_s (1-\epsilon) A_g} \tag{9}$$

where $A_g$ is the geometrical cross-sectional area of the fluidized bed.

For Test RIA 1-4, $A_g = 13.48$ cm$^2$, Equation 9 can then be rewritten as

$$B_{R_e} = 325.3 \quad \frac{\xi \; Q_B}{\alpha \phi_s (1-\xi)} \tag{10}$$

In equation 10, $Q_B$ is the shroud inlet flow to the fluidized bed in terms of (cm$^3$/s). For Test RIA 1-4, assume $\xi$ to be 0.1, $\phi_s = 0.8$, $\alpha = 20$, and

$Q_B = 383$ cm$^3$/s and $B_{R_e}$ therefore is 778.

Thus the pressure drop in the rubble bed can be approximated by using the Burke-Plummer[5] equation as,

$$\frac{\Delta P}{L} = 1.75 \quad \frac{\rho_c V_o^2}{D_P} \frac{\xi}{(1 - \xi)^3} \tag{11}$$

The coolant volumetric flow through the rubble bed, $Q_B$, is given as

$$Q_B = V_o \, Ag \, (1-\xi) \tag{12}$$

where Ag is the actual geometrical area of the bundle ( 13.48 cm$^2$). Eliminating $V_o$ between equations 11 and 12 we obtain the following simplified expression for the pressure gradient across the flow shroud.

$$\frac{\Delta P}{L} = 7.564 \times 10^{-3} \frac{Q_B^2}{D_P} \frac{\xi}{(1-\xi)^5} \quad (13)$$

For a constant pressure gradient across the shroud, before and after the burst, the flow blockage due to fuel fragmentation and relocation can be assessed by comparing the shroud coolant flow measurements made before and after the burst. Eliminating ($\Delta P/L$) between equations 4 and 13 gives the ratio of the coolant flow through the shroud after the burst to that before the burst in terms of the flow blockage in the debris beds, and the average debris particle diameter, $D_p$:

$$\frac{Q_B}{Q} = 0.164 \left[\frac{D_P}{Q^{0.25}} \frac{(1-\xi)^5}{\xi}\right]^{1/2} \quad (16)$$

Examination of Equation 16 indicates that the ratio ($Q_b/Q$) should be less than one if a rubble bed had formed in the fuel bundle after the power burst. Figure 19, however, shows an increase in the shroud flow from the measurements made five hours after the power burst relative to the pre power burst measurements. Fuel particle washout in the five hour interval may have occurred which reduced the flow restriction within the shroud. A 50% reduction in the shroud coolant flow was observed about 20 s after the burst indicating the occurrence of flow blockage by the break-up and fragmentation of the fuel. This time is about 10 s after the cladding quench time indicated by the cladding surface thermocouples. Hot cell examination of the bundle will be performed to characterize the fuel rod failure and extent of the flow blockage.

## 6. FISSION PRODUCT DETECTION SYSTEM RESULTS

Two minutes and 50 seconds following the power burst a sharp rise in fission product activity was observed in the loop coolant sample line monitored by the FPDS. This delay was expected due to the transport of the

coolant from the test train to the FPDS. At least one and probably several of the test rods failed during the power excursion. Delayed neutron activity was not observed; either the detector failed, or delayed neutron activity was below the minimum detectable level. The gross gamma signal decayed below minimum sensitivity approximately one hour following the initial response.

Using the 5 cm collimator aperature, the spectrometer was able to analyze a 500 cps gamma field for 12 hrs. after the power burst and, thus, collect useful spectra for fission product behavior analysis. Spectra were collected at 15 second intervals during the first 20 minutes following the burst, and graduated to 10 minute intervals at later times. The predominate isotopes identified in the quick look analysis were Kr-87 & 88, Rb-88 & 89, Te-132, I-131, 132, 133, 135, Xe-135 & 138, and Cs-137 & 138. Of particular interest is the $^{137}Cs$ which has a half-life of 30.2 years. The detection of this important long lived species in the presence of considerable short lived isotopes is a useful capability not previously demonstrated by the FPDS.

## 7. SUMMARY OF RESULTS AND DISCUSSION

The primary objective of Test RIA 1-4 was to provide information regarding loss-of-coolable fuel rod geometry following a RIA event for a peak fuel enthalpy equivalent to the present NRC licensing criteria of 280 cal/g $UO_2$. The following results and observations are based on evaluations of the preliminary data. Final information and conclusions regarding the objective of the test must await post-irradiation examination of the 9-rod bundle and qualification of the on-line data.

1. Based on the average data of the four core power chamber and one of the test train neutron flux detectors, a radially-averaged peak fuel enthalpy of 281 cal/g $UO_2$ was attained for the corner fuel rods; the test objective was 280 cal/g $UO_2$. Final energy data will be based on fuel burnup results and qualified on-line data.

2. The maximum measured cladding surface temperatures were about 500 K lower than the predicted and the time in film boiling was considerably less than that predicted.

3. The maximum measured pressure pulse ($\sim$1.9 MPa) was about the same as that predicted. The pressure pulse is believed to be caused by the rapid heating of the coolant due to direct $\gamma$ and neutron heating during the power burst.

4. The general thermal hydraulic behavior of the RIA 1-4 bundle was different than that observed in previous separately shrouded single fuel rod RIA tests. The flow excursion out of the shroud due to gamma and neutron prompt heating of the coolant during the burst induced voiding of about 25% of the shroud coolant for more than 0.5 s. Flow stagnation occurred from about 0.2 to 0.7 s following the power burst and then the shroud flow gradually increased to the pre power burst flow rate. At 20 s after the power burst, the flow rapidly decreased to about 50% of the pre power burst shroud flow rate. Fuel washout may have occurred in the five hour interval before flow bypass measurements could be made after PBF reactor building re-entry could be accomplished.

5. Complete flow blockage such as was observed for the two irradiated fuel rods in Test RIA 1-1 did not occur for Test RIA 1-4. Partial flow blockage occurred as evidenced by the approximately 50% reduction in the shroud flow rate about 20 s after the time of peak power. The flow area per fuel rod was about 15% larger for Test RIA 1-4 than for the individually shrouded rods in Test RIA 1-1, while the average rod peak fuel enthalpy was about 8% less for Test RIA 1-4 than for Test RIA 1-1. Both of these factors would tend to reduce the tendency for flow blockage in Test RIA 1-4 as compared to Test RIA 1-1.

## 8. REFERENCES


1. Division of Reactor Safety Research, Office of Nuclear Regulatory Research, United States Nuclear Regulatory Commission, Water Reactor Safety Research Program, A Description of Current and Planned Research, NUREG-0006, February 1979.

2. C. J. Stanley, Z. R. Martinson, Reactivity Initiated Accident Test Series, Test RIA 1-4 Experiment Operating Specification, TFBP-TR-323, June 1979.

3. S. J. Seiber and T. E. Young, Physics Calculations for the RIA 1-4 9-Pin Test, RE-P-79-047, July 1979.

4. S. K. Fukuda and Z. R. Martinson, Reactivity Initated Accident Test Series, Test RIA 1-4 Experiment Predictions, EGG-TFBP-5023, February 1980.

5. R. B. Bird, et al., Transport Phenomena, John Wily & Sons Inc. (1960).